Conditioning by Subthreshold Synaptic Input Changes the Intrinsic Firing Pattern of CA3 Hippocampal Neurons

Saray Soldado-Magraner[13]*, Federico Brandalise[23], Suraj Honnuraiah[1], Michael Pfeiffer[1], Urs Gerber[2], Rodney Douglas[1]

[1]*Institute of Neuroinformatics, University of Zurich and ETH Zurich, Switzerland*
[2]*Brain Research Institute, University of Zurich, Switzerland*
[3]*These authors contributed equally to this work*
Correspondence: ssaray@ini.uzh.ch, rjd@ini.uzh.ch

1 Abstract

2 Unlike synaptic strength, intrinsic excitability is assumed to be a stable property of neurons. For example, learning of

3 somatic conductances is generally not incorporated into computational models, and the discharge pattern of neurons

4 in response to test stimuli is frequently used as a basis for phenotypic classification. However, it is increasingly

5 evident that signal processing properties of neurons are more generally plastic on the timescale of minutes. Here we

6 demonstrate that the intrinsic firing patterns of CA3 neurons of the rat hippocampus in vitro undergo rapid long-term

7 plasticity in response to a few minutes of only subthreshold synaptic conditioning. This plasticity on the spike-timing

8 could also be induced by intrasomatic injection of subthreshold depolarizing pulses and was blocked by kinase

9 inhibitors, indicating that discharge dynamics are modulated locally. Cluster analysis of firing patterns before and

10 after conditioning revealed systematic transitions towards adapting and intrinsic burst behaviours, irrespective of the

11 patterns initially exhibited by the cells. We used a conductance-based model to decide appropriate pharmacological

12 blockade, and found that the observed transitions are likely due to recruitment of calcium and M-type potassium

13 conductances. We conclude that CA3 neurons adapt their conductance profile to the subthreshold activity of their

14 input, so that their intrinsic firing pattern is not a static signature, but rather a reflection of their history of subthreshold

15 activity. In this way, recurrent output from CA3 neurons may collectively shape the temporal dynamics of their

16 embedding circuits.

New & Noteworthy

Despite being widely conserved across the animal phyla, it is still a mystery why nerve cells present diverse discharge dynamics upon somatic step currents. Adding a new timing dimension to the intrinsic plasticity literature, here we show that CA3 neurons rapidly adapt through the space of known firing patterns in response to the subthreshold signals that they receive from their embedding circuit. This result implies that CA3 neurons collectively adjust their network processing to the temporal statistics of their circuit.

Keywords

Firing patterns, intrinsic plasticity, subthreshold plasticity, neurocentric learning, somatic conductance tuning, spike-timing modulation, CA3 hippocampus.

Introduction

Neurons of the Central Nervous System present an intriguing diversity of firing patterns in response to applied intra-somatic step currents (McCormick et al., 1985; Connors and Gutnick, 1990; Cauli et al., 2000; Markram et al., 2004; Butt et al., 2005; Dumitriu et al., 2007; Hemond et al., 2008; Somogyi and Klausberger, 2005; Tasic et al., 2016). These responses may be for example: adapting, accelerating, bursting or fast spiking, but why neurons have evolved these diversity of precise spike-timings remains an open issue. With some exceptions (Steriade, 2004), the patterns are assumed to be a sufficiently stable property of a neuron to be used as a basis for phenotypic classification (Markram et al., 2004; Ascoli et al., 2008; Tricoire et al., 2011; Van Aerde and Feldmeyer, 2015).

However, there are substantial reasons to doubt that firing patterns are static properties of neurons. The discharge dynamics depends on the distribution and activations of the membrane conductances that it expresses (Hille, 2001; Markram et al., 2004). This distribution is subject, over the course of hours and days, to homeostatic control via up- or down-regulation of conductances in response to the neuron's own activity (Turrigiano et al., 1994; Turrigiano and Nelson, 2004; Marder and Goaillard, 2006). Furthermore, neurons have conserved molecular pathways that link network activity to the recruitment of genes and signaling factors implicated in neural excitability (Flavell and

Greenberg, 2008; Cohen and Greenberg, 2008), and activity-dependent maturation is necessary for the emergence of the whole spectrum of electrical types (Moody and Bosma, 2005; García et al., 2011). These lines of evidence suggest that the firing pattern is not a static characteristic of the cell, but rather the consequence of adaptive mechanisms that adjust the spike-timing of the neuron in response to the patterns of activity in its embedding network. In fact, some studies show that specific features of the discharge response are actually modulated homeostatically upon activity or after learning. For example, the spike delay (Cudmore et al., 2010; Dehorter et al., 2015) or the accommodation rate (Thompson et al., 1996).

Changes in intrinsic excitability have recently been reported also on faster time scales (Aizenman and Linden, 2000; Paz et al., 2009; Mahon and Charpier, 2012; Brager and Johnston, 2007). These shifts are postulated to increase the probability of firing, integrating neurons into memory engrams in synergy with hebbian learning (Zhang and Linden, 2003; Titley et al., 2017). However, the fact that key conductances with potential impact on the spike pattern have also been found to be rapidly modulated by activity (Belmeguenai et al., 2010; Hyun et al., 2013; Brown and Randall, 2009; Grasselli et al., 2016) suggests neurons may be doing more than just increasing their overall excitability, for instance, adjusting their temporal processing as well (Debanne et al., 2019). Despite the evidence, it remains unexplored whether neurons can rapidly modulate upon activity not just specific features of the discharge or its average rate, but the whole spectrum of intrinsic spike-timings classically described (Ascoli et al., 2008).

We have addressed this issue by studying the effect that subthreshold activity has on the suprathreshold response of neurons using whole-cell recordings in the CA3 region of the rat hippocampus in organotypic cultures. The discharge patterns were characterized before and after a conditioning phase of periodic subthreshold synaptic stimulation lasting a few minutes. Pre-conditioned cells presented diverse discharge patterns (Ascoli et al., 2008). However, conditioning by subthreshold synaptic input elicited significant long-lasting changes in the behavior of most of the neurons examined, requiring substantial re-classification of their type. This effect was reproduced when conditioning the cells via subthreshold intra-somatic current pulses and was blocked by adding protein kinase A (PKA) and protein kinase C (PKC) inhibitors to the recording pipette, suggesting that changes are mediated at the single cell level via phosphorylation. The conditioning effect was also reproduced in juvenile mice using the acute slice preparation technique, indicating

3

65 it is a generic property of CA3 cells. Using a conductance-based neuron model and the channel blockers XE991 and

66 $NiCl_2$ we found that the results can be explained by a recruitment of voltage dependent calcium and M-type potassium

67 conductances. We conclude that CA3 neurons rapidly adapt their spike-timing response by tuning their conductance

68 profile to the subthreshold inputs of their embedding circuit.

Results

Firing patterns of CA3 neurons change after subthreshold synaptic stimulation

71 Whole-cell patch clamp recordings of CA3 neurons were performed in rat hippocampal organotypic cultures. The

72 intrinsic firing patterns of the neurons were recorded before and after conditioning by extracellular stimulation of

73 the mossy fibers (MF) originating in the dentate gyrus. The conditioning stimuli consisted of paired pulses (0.1

74 ms duration pulses, with an interval of 10 – 20 ms) applied at 1 Hz, and repeated 500 times for a total period of

75 approximately 8 minutes. The amplitude of the pulses was adjusted for each recorded cell to elicit only subthreshold

76 excitatory post-synaptic potentials (EPSPs). This mossy fiber stimulation protocol is a modification of that described

77 by Brandalise and Gerber (2014) and Brandalise et al. (2016), which has been previously shown to elicit heterosynaptic

78 subthreshold plasticity in CA3 pyramidal-pyramidal synapses. We tested whether the same type of subthreshold

79 stimulation could also induce plasticity on the action potential discharge patterns of the CA3 cells. The firing patterns

80 of neurons were assessed with a sequence of constant current injections. For convenience, we label these patterns

81 according to the Petilla classification terminology (Ascoli et al., 2008). Interestingly, we observed that for most

82 neurons the conditioning protocol elicited a change in the Petilla discharge pattern, independently of their type of

83 firing on control conditions. For example, the pyramidal cell shown in Figure 1A had a non-adapting burst pattern

84 before stimulation (grey traces) but after conditioning (blue traces), this response changed to intrinsic burst. The same

85 transition was observed for the pyramidal cell on Figure 1B, whose initial pattern was delayed accelerating. The

86 bipolar cell on Figure 1C switched from non-adapting continuous to adapting continuous firing. The most common

87 transition was towards adapting and intrinsic burst patterns. This observation is supported by measuring the mean

88 fraction of spikes in the first half versus the second half of the voltage traces for the population of recorded cells. The
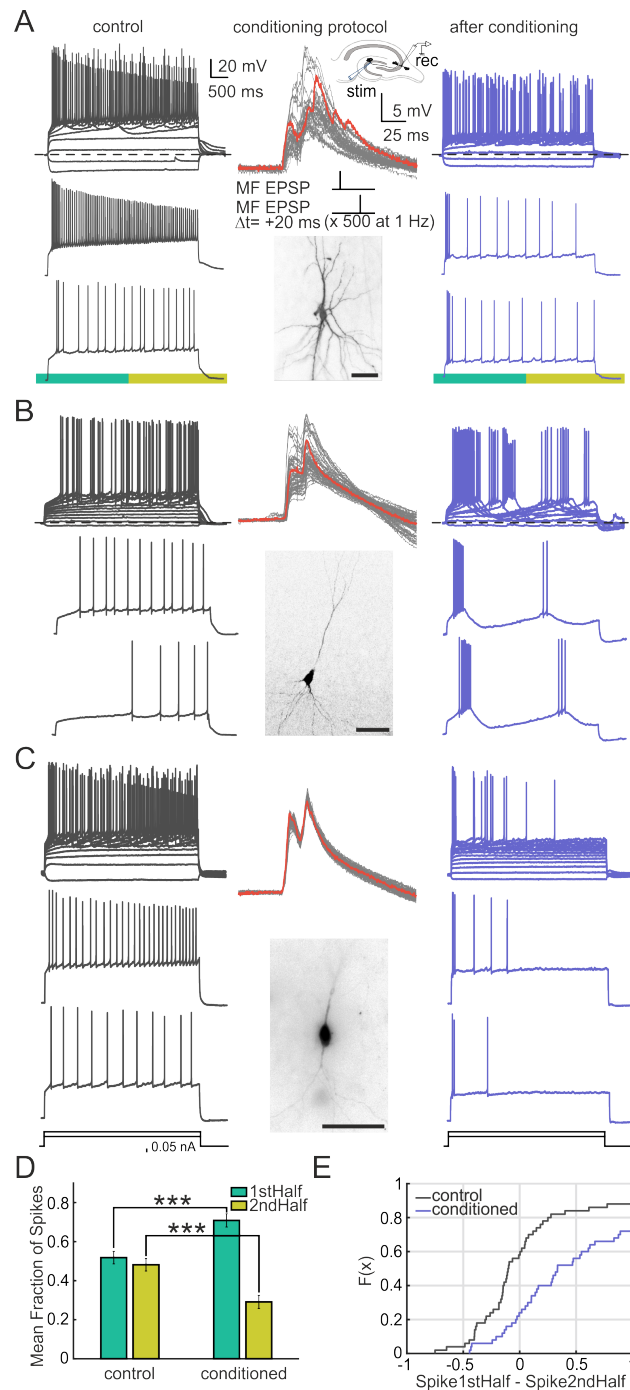
Figure 1. Firing pattern transitions occur in CA3 neurons after subthreshold paired-pulse stimulation of afferents. A-C) Three examples of neurons in the CA3 area presenting different morphologies and different firing patterns in control conditions. The discharge patterns were measured by injection of step currents of increasing amplitude. Control measurements (grey traces, left) were followed by stimulation of the mossy fibers. The upper trace shows all voltage traces elicited upon different levels of current injection on that cell. Two sample traces of this set are shown below. EPSPs (middle panel) were evoked in response to a stimulation with double current pulses, separated by 20 ms and repeated 500 times at 1 Hz. The series of repeated pulses are shown superimposed. The median trace is highlighted in red. The inset shows the configuration of recording and stimulating electrodes (on the CA3 region of the hippocampus and on the dentate gyrus, respectively). Below, the morphology obtained by labelling the cells with biocytin is shown. After the conditioning, patterns were measured again (blue traces, right). A) Pyramidal cell switches from non-adapting burst to intrinsic burst firing. B) Pyramidal cell switches from delay accelerating to intrinsic burst continuous pattern. C) Bipolar cell switches from non-adapting continuous to adapting continuous firing (scale bars = 50μm). D) Mean fraction of spikes for the population in the first and second half of the voltage trace (see green and yellow rectangle below the trace in A for an example) for both control and conditioned cases. A significant redistribution on the fraction of spikes is observed after the conditioning, where the fraction of spikes on the first half is increased while it decreases in the second half (n=50, p=1.92e-6, two-sided Wilcoxon signed rank test). E) Empirical cumulative distribution function for the data shown in D. Every individual cell, for both control and conditioned cases, is represented as the number of spikes for the first half of the trace minus the spikes for the second half (n=50)

distribution of the spikes favors the first half (Figures 1D-E) (n=50), supporting our observation that the main pattern

transitions are towards adapting and intrinsic burst behaviors after the conditioning.

The mossy fiber conditioning was followed by a significant 36 MΩ (25%) decrease in input resistance (Rin), (from

144.8 ± 73.0MΩ to 108.4 ± 65.3MΩ, two-sided Wilcoxon signed rank test, p=1.1e-5), while there was no significant

change in rheobase (from 0.36 ± 0.32 nA to 0.3 ± 0.6 nA, two-sided Wilcoxon signed rank test, p=0.59). There was

also a significant 5 mV (7%) depolarization of the resting membrane potential (Vm) (-65.3 ± 5.0mV) with respect

to resting level (-70.4 ± 5.7mV, two-sided Wilcoxon signed rank test, p=2.3e-5, n = 50). However, the firing pattern

transitions could not be induced by simply clamping the membrane potential at different values (see Figure S1D and

F, n = 10), nor could they be induced by the step-currents used to measure the discharge patterns (see Figure S1A-C,

n = 15). No significant changes in Vm or Rin were found in unconditioned cells (Vm: -69.3 ± 2.0mV, -69.1 ± 1.9mV,

paired t-test, p=0.64, Rin: 148.8 ± 56.1MΩ, 158.9 ± 55.6MΩ, paired t-test, p=0.063, n = 15). Intracellular dialysis

could also be excluded as the cause of the pattern transitions, as firings did not change spontaneously over intracellular

recording time (see Figures S1D and F). In addition, a change in the fraction of spikes in favor of the first half was also

found after conditioning in a setting where dialysis was minimized (high resistance pipette recordings, 10-12 MΩ,

n=10, p=0.048, two-sided Wilcoxon signed rank test).

We noted however a significant change in the mean fraction of spikes (in favor of the first half) after 20 min of

recording, when assessing the firing pattern three times during this period (n = 12, p=0.005, two-sided Wilcoxon

signed rank test). This indicates that transient suprathreshold current steps can also trigger changes in firing, as

previous studies in CA3 have reported (Brown and Randall, 2009), although continuous subthreshold conditioning

over a shorter time scale has a stronger effect (8 minutes, Figure 1).

Firing pattern transitions are gradual during the course of the conditioning and long-lasting

We next assessed whether the expression of the firing transition was gradual or whether firings changed more sharply

during the course of the conditioning. To this end, we repeated the original experiment (Figure 1) while assessing the

firing pattern of the cells every 100 trials of conditioning. The general observation was that cells displayed a gradual
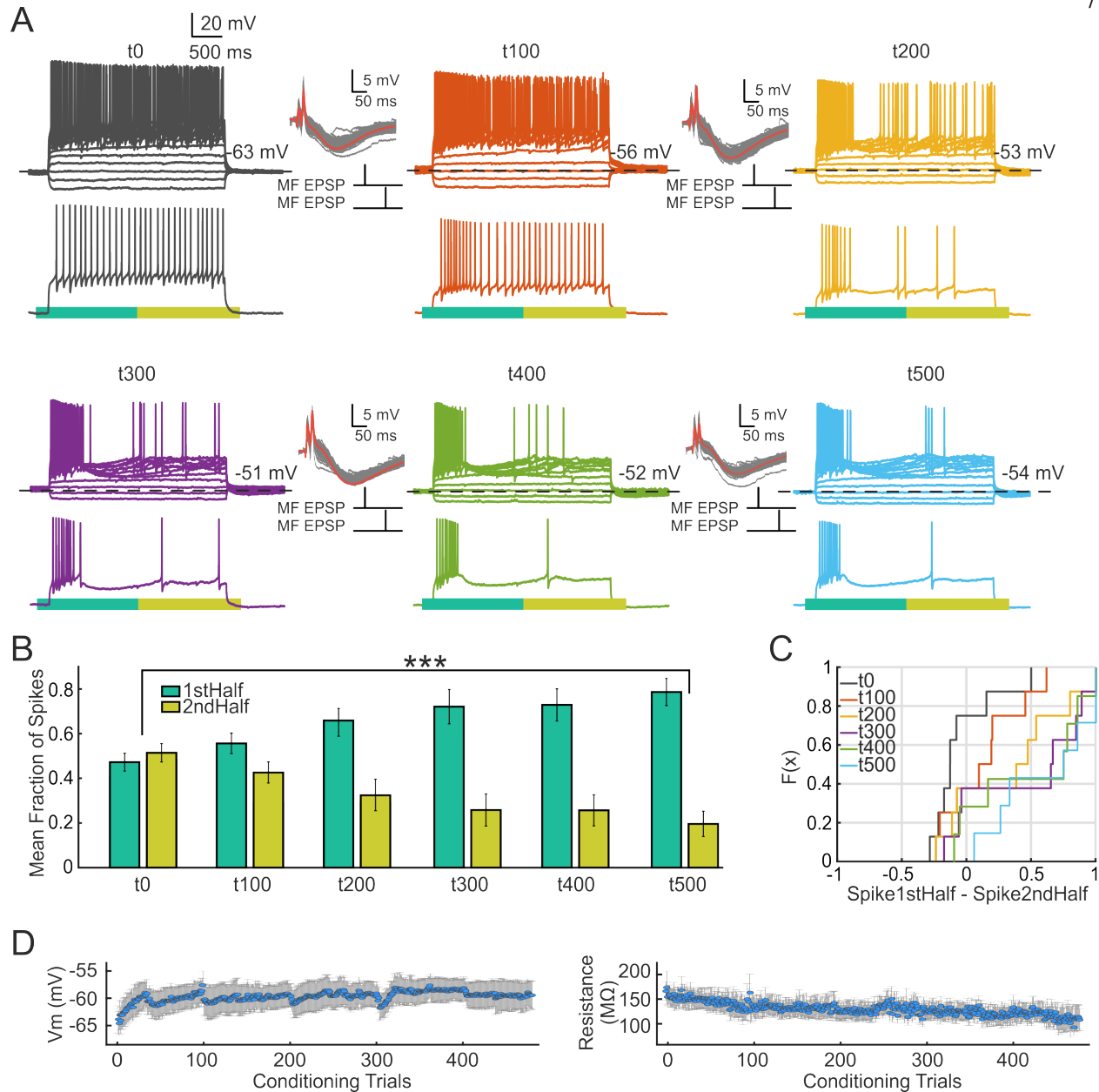
Figure 2. The expression of the conditioning effect is gradual over the course of the stimulation. Firing patterns were assessed every 100 conditionings until 500 trials were completed. A) Representative cell whose firing pattern is non-adapting in control conditions (grey). After 100 stimulations the cell shows an adapting pattern (red), after 200 the adaptation gets stronger and an intrinsic burst pattern emerges after the successive conditionings (orange to blue). Conditioning protocols are showed on the insets. Red line shows the median. B) Mean fraction of spikes for the population in the first and second half of the voltage trace during the successive conditionings. A significant redistribution on the fraction of spikes is observed during the course of the conditioning. The fraction of spikes on the first half continuously increases in favor of the second half (n = 8, p=1.24e-5, repeated measures ANOVA) C) Empirical cumulative distribution function for the data shown in B. The number of spikes for the first half of the trace minus the spikes for the second half is shown for every cell (n=8) D) Average resting membrane potential (Vm) and input resistance (Rin) of the cells during the course of the conditioning. Vm was measured as the baseline voltage before the depolarization caused by the conditioning, Rin was measured by injecting a negative current step after each conditioning trial. Circles indicate mean, bars indicate SEM (n=8). In the cases where Vm was above -60 mV a small holding current was injected to keep the cell stable during the conditioning.

transition in firing, in which more regular or accelerating patterns changed towards different degrees of adaptation and intrinsic burst responses. For example, the cell shown in Figure 2A presents a non-adapting or regular pattern in control conditions. After 100 repetitions of the conditioning protocol the spike distribution changes to an adapting continuous pattern. This adaptation gets reinforced after 200 conditionings, with the cell later adopting an intrinsic burst pattern. Other cells showed a progression for more regular to only adapting patterns. As an average, the smooth transition is reflected in the mean fraction of spikes shown in Figures 2B and C. As it can be observed, successive conditionings translate into a stronger redistribution of this fraction in favor of the first half of the trace, a reflection of the cells adopting a stronger adapting or intrinsic burst responses (n=8). The progression of the resting membrane potential (Vm) and input resistance (Rin) during the course of the conditioning was also monitored, and it is shown in Figure 2D. A progressive increase in Vm and a progressive decrease in Rin is observed (Rin, from $166.4 \pm 54.2M\Omega$ to $115.3 \pm 53.3M\Omega$, two-sided Wilcoxon signed rank test, p=0.031, n=7) (Vm, from $-64.6 \pm 6.2mV$ to $-58.7 \pm 5.7mV$, two-sided Wilcoxon signed rank test, p=0.047, n = 7).

Changes in intrinsic properties of neurons have been previously reported to be long-lasting, similar to synaptic forms of long-term plasticity (Turrigiano and Nelson, 2004; Titley et al., 2017). We thus assessed whether the firing pattern plasticity was stable in time or whether the changes were transient. We conditioned the cells and followed their firing response up to 30 minutes after conditioning. In all cases, cells presented a post-conditioned characteristic change in firing pattern towards adapting and intrinsic burst patterns (as in Figure 1). This same pattern was assessed every 10 minutes and showed to be persisting up to the whole recording period (see Figure 3), indicating a long-lasting change in intrinsic excitability. In two cells the pattern persisted up to 50 min of recording. A representative cell is shown in Figure 3A, which presented an accelerating pattern that switched to intrinsic burst after conditioning. This induced pattern remained stable for 30 min. At the population level, the stability is reflected in the mean fraction of spikes. After the conditioning effect, no significant change in this fraction was observed over 30 min (see Figure 3C)(n=6). Note that for this subset of cells a 60 ms paired pulse was employed during the conditioning (see Figure 3A). The previous observed changes in firing occurred upon conditioning with a paired mossy fiber current pulse separated by 20 ms and given at a frequency of 1 Hz (Figure 1). We wondered whether a different timing interval (60 ms) would

138 affect the outcome of the conditioning, as shown by previous reports of subthreshold synaptic plasticity in the CA3

139 circuit (Brandalise and Gerber, 2014; Brandalise et al., 2016). However, no differential effect on the pattern was found

140 (Figure 3), indicating that the mechanism of intrinsic firing plasticity is not sensitive to these two different time scales.

Firing pattern transitions are independent of synaptic input and are blocked by protein kinase A and C inhibitors

142 We attempted to resolve whether synaptic input was necessary to elicit the changes, or whether they could be induced

143 by direct stimulation of the soma. To this end, we used intra-somatic injection of paired step current pulses whose

144 parameters were chosen to elicit a similar somatic voltage response compared to that generated by the mossy fiber

145 stimulation (Figure 4). This direct subthreshold somatic stimulus evoked changes in discharge pattern that were

146 similar to those elicited by the indirect mossy stimulation. For example, the cell in Figure 4A displayed a delay

147 accelerating firing pattern in control conditions and underwent a transition towards intrinsic burst pattern after somatic

148 conditioning. The population data for direct stimulation showed a significant redistribution in the fraction of spikes

149 in favor of the first half of the trace versus the second half after the conditioning (Figures 4B and C) (n=12). In these

150 experiments we observed the same tendency of neurons to become adapting and intrinsic burst after conditioning as

151 for mossy fiber stimulation. This result suggests that the mechanism underlying the changes in firing pattern is not

152 localized to synapses, but rather acts at a more central, probably somatic or proximal dendritic level.

153 The fact that the firing pattern transitions could be reproduced by this direct depolarization of the soma raised the

154 question of whether the somatic depolarization elicited by mossy fiber activation is necessary to elicit the observed

155 changes in firing. We thus repeated the mossy conditioning experiment (Figure 1) while artificially hyperpolarizing

156 the neuron (see Figure S2). The hyperpolarization did not abolish the effect of the conditioning, since a significant

157 redistribution of spikes in favor of the first half of the trace was observed after the conditioning (see Figure S2B and

158 C). However, the effect was stronger when conditioning the cells without hyperpolarization (see Figure S2B or Figure

159 1D for comparison). An example cell is shown in Figure S2A. The cell presents an accelerating pattern in control

160 conditions. After conditioning via the mossy fiber pathway, under the presence of an hyperpolarizing pulse, the cell

161 changed its firing towards a non-adapting burst pattern. When re-conditioning the cell with no hyperpolarization the
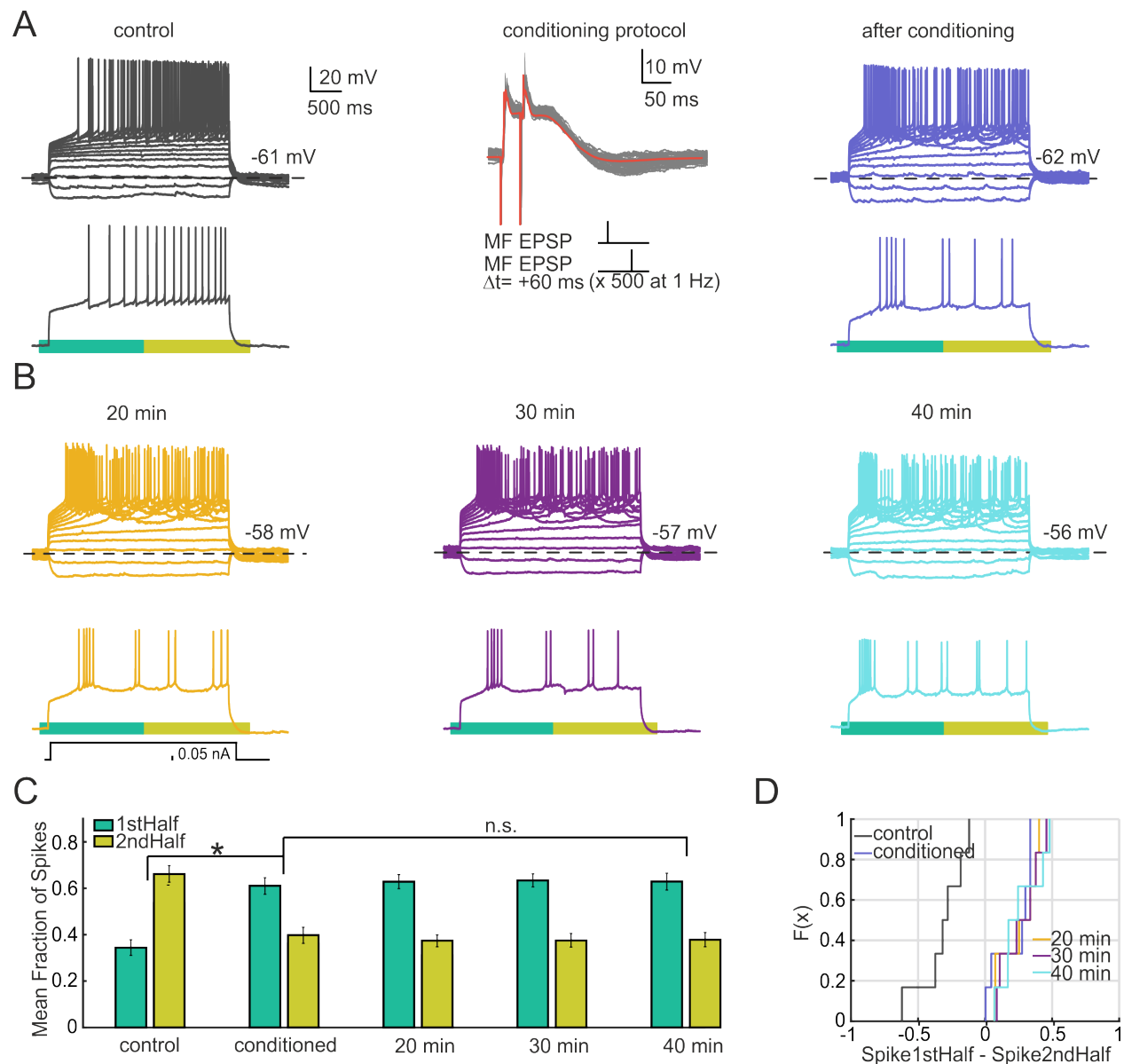
Figure 3. The effect of the conditioning is persistent over time. Cells where followed for 40 minutes to assess whether the firing pattern plasticity was long-term. A) Example cell with an accelerating firing pattern in control conditions (grey). The cell was conditioned subthresholdy with a double mossy fiber current pulse separated by 60 ms and given at a frequency of 1 Hz (protocol is shown in the middle, red line indicates the median). A change in pattern to intrinsic burst is elicited (blue). B) The same cell was followed every 10 min after conditioning until reaching 40 min of recording (orange, purple and blue). The pattern remained stable. C) Mean fraction of spikes for the population in the first and second half of the voltage trace before, after conditioning and every 10 min thereafter. A significant redistribution on the fraction of spikes is observed after the conditioning (n=6, p=0.031, two-sided Wilcoxon signed rank test). No significant change in this fraction was observed over 30 min after conditioning (n=6, p=0.4, repeated measures ANOVA). D) Empirical cumulative distribution function for the data shown in C.
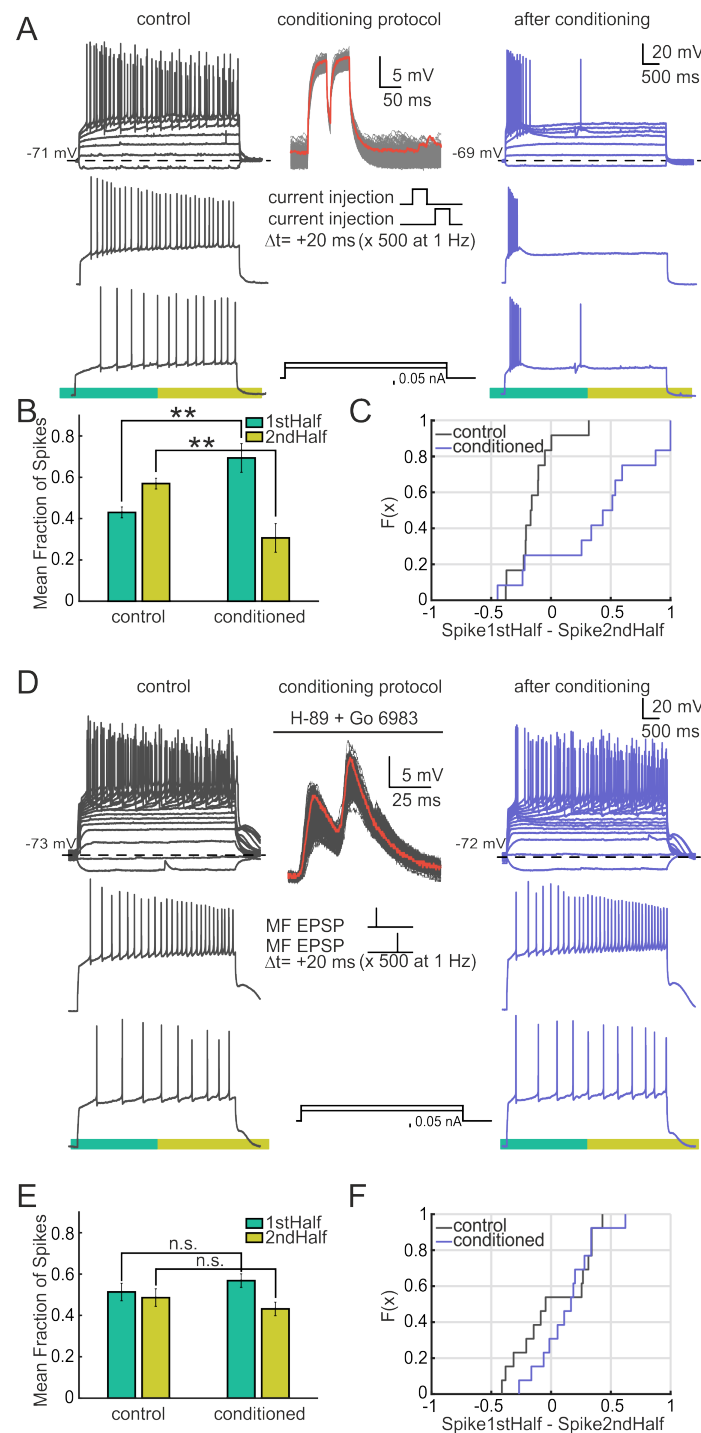
Figure 4. CA3 firing pattern transitions occur upon somatic conditioning and are blocked by kinase inhibitors. A) Example of an intrasomatic conditioned cell that switched from delay accelerating (grey traces) to intrinsic burst firing (blue traces). The conditioning protocol is shown in the middle column. The red line shows the median. EPSPs were evoked by injection of paired current steps, of 50 ms in duration and separated by 20 ms. The double steps were repeated 500 times at 1 Hz. The series of repeated pulses are shown superimposed. A sample trace is shown in red. B) Mean fraction of spikes for the population in the first and second half of the voltage trace for both control and conditioned cases. A significant redistribution on the fraction of spikes occurs after the conditioning. The fraction of spikes on the first half is increased while it decreases in the second half (n=12, p=0.0024, two-sided Wilcoxon signed rank test). C) Empirical cumulative distribution Function for the data shown in B. Every individual cell is represented as the number of spikes for the first half of the trace minus the spikes for the second half (n=12). D) Example of a mossy fiber conditioned cell (as described in Figure 1) under the presence of H-89 and Go 6983 (PKA and PKC inhibitors) on the intracellular pipette. The cell expresses a delay accelerating pattern in control conditions and remains under such pattern after the conditioning protocol is applied. E) Mean fraction of spikes for the population in the first and second half of the voltage trace for both control and conditioned cases. The redistribution of the fraction of spikes was not significant after the conditioning (n=13, p=0.266, two-sided Wilcoxon signed rank test). F) Empirical cumulative distribution function for the data shown in D. Every individual cell is represented as the number of spikes for the first half of the trace minus the spikes for the second half (n=13).

162 pattern switched to intrinsic burst. These results suggest that a transient depolarization, such as the intrasomatically

163 injected stimulus, is sufficient but not necessary to elicit the effect. The residual effect may indicate that the mechanism

164 is localized near the MF synapse, in which case somatic hyperpolarization could be insufficient to prevent depolarization

165 there. Note however that in most neurons a handful of depolarizing trials were accidentally elicited while adjusting

166 the magnitude of the current MF pulse. Additionally, some cells presented occasional rebound spiking caused by the

167 hyperpolarization, while an increase in stimulation amplitude due to the increase in driving force was also frequent.

168 This could all potentially contribute to the observed effect.

169 Next, we sought to identify what internal mechanism could be responsible for the firing pattern transitions. The firing

170 pattern of the cell depends on the distribution of ion channels, or conductances, that the cell presents at its membrane

171 (Hille, 2001). A possible mechanism would act by changing this distribution. Due to the time scale of the response

172 (on the order of minutes) we ruled out protein synthesis of new channels on the membrane. An alternative could

173 be channel phosphorylation, a mechanism known to affect the maximal conductance of the channel on a relatively

174 short timescale (Davis et al., 2001). We reproduced the conditioning protocol in the presence of the PKA and PKC

175 inhibitors H-89 and Go 6983 in the intracellular recording pipette. Figure 4D shows a cell whose firing pattern in

176 control conditions was delay accelerating. After mossy fiber conditioning in the presence of the inhibitors the cell

177 retained this initial pattern. 84% of cells recorded with phosphorylation inhibitors showed no visible modulation of

178 the Petilla label pattern (11 out of the 13 cells). Figures 4E and F show the population response for these cells. Unlike

179 Figure 1D, no significant redistribution of the spikes was found on the presence of the inhibitors (n=13). These results

180 suggest that phosphorylation is implicated in the mechanism of firing pattern transition.

181 Using Dynamic Time Warping (DTW) and a conductance based model to infer firing transitions and parameter

182 changes after plasticity

183 We observed that the conditioning induced firing pattern changes from more regular patterns towards early bursting

184 and adapting patterns. We sought to quantify these changes using hierarchical clustering methods (Druckmann et al.,

185 2013; Tricoire et al., 2011; Hosp et al., 2014) to establish more objectively which discharge type to associate with

12

186 every response, and to quantify the frequencies of transitions between them. For our clustering method, we obtained

187 instantaneous firing rate vectors of the experimental voltage traces and estimated pairwise distances using the DTW

188 algorithm. DTW operates directly on the action potential temporal sequence rather than relying on a pre-defined set

189 of features (Druckmann et al., 2013; Tricoire et al., 2011; Hosp et al., 2014). The rate vectors used for the clustering

190 can be interpreted as the subthreshold voltage envelope in which the discharge response of each cell rides, and this

191 envelope is the essence to catalogue similar firing patterns. Once the distances between the vectors were calculated,

192 Wards linkage was applied in order to obtain a hierarchical tree to reveal the classes.

193 The results of the cluster analysis of discharge patterns are shown in Figure 5A. We set the threshold of the clustering

194 tree at a level that separates the traces into 5 distinct families. The threshold was chosen large enough to yield sufficient

195 structure to interpret the hierarchy in terms of recognized response types (Ascoli et al., 2008). Representative traces

196 of each family are shown in Figure 5B. The average of the firing rate vectors of every cluster is depicted beneath each

197 representative trace.

198 The clustering algorithm successfully captures the typical time courses of the firing patterns. The right branch of

199 the cluster tree contains accelerating and non-adapting firing patterns, while the other contains adapting and intrinsic

200 bursting patterns together with a smaller group of traces that have delayed spiking profiles. The consistency of the

201 algorithm was confirmed by its successful clustering of independent rate vectors derived from the same set of current

202 injections (same cell under the same conditions) into a single cluster. Indeed, in 86% of cases (43 of the 50 cells) the

203 algorithm successfully allocated the majority of vectors from the same set of current injections into single clusters.

204 Vectors from the 7 remaining cells were not consistently classified. For 50% of the cells all of their voltage traces

205 fell into the same cluster, and for 90% of the cells at least 50% did. The allocation of some responses from the

206 same cell into more than a single cluster does however follow a biological logic. For example, for cells classified as

207 accelerating, some of their voltage traces could reasonably fall into the non-adapting cluster because acceleration may

208 vanish at high current injections. A similar reasonable misclassification is possible for adapting traces. In this case

209 low current injections may be classified as non-adapting because the currents are not high enough to elicit adaptation.

210 In particular, many of the traces belonging to the delayed spiking cluster are derived from cells whose traces at low

13
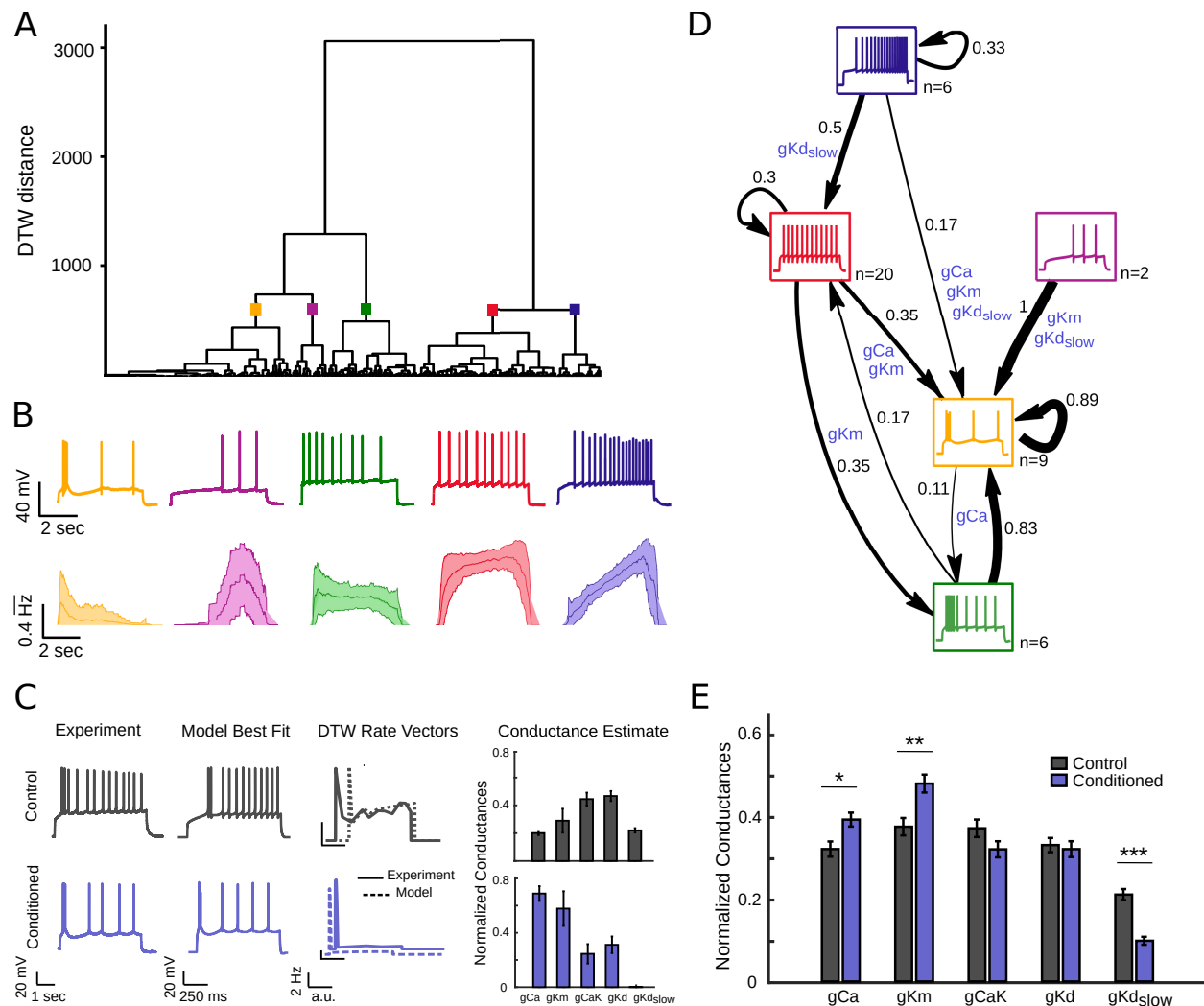
Figure 5. Hierarchical clustering of experimental discharge traces and mapping to a conductance model. A) Dendrogram of clustered traces. The data included in the cluster corresponds to the mossy fiber conditioned cells of Figure 1. Two main families can be identified: one containing adapting and bursting traces, together with delayed spiking patterns (left branch); and another branch containing regular and accelerating traces (right branch) (n=50). B) Representative traces from each cluster. Below, average instantaneous firing rate over all traces belonging to the same cluster. Middle lines indicate the mean; light outer lines indicate standard deviations. The instantaneous firing rate (in Hz) is normalized to 1. C) Every experimental trace is matched to a model database of traces. Using the DTW distance on the instantaneous firing rate vectors the best matches are selected (best match is depicted). A conductance estimate for the experimental trace is obtained (average of 10 best matches are shown). D) Transitions observed between firing patterns before and after conditioning. Each cell is assigned to a single cluster (represented as a box) for both the control and conditioned cases. Arrows indicate transitions between types whenever a cell changed cluster. Self-loops indicate that the firing pattern was retained after conditioning. Numbers indicate percentages of observed transitions. The number of cells in each category under control conditions is displayed next to each pattern type. Cells tend to transition towards adapting and bursting patterns following conditioning (n = 43). Seven cells were assigned as unclassified. A conductance road map showing the key conductances responsible for a transition in firing pattern are represented on the edges. The main channels implicated are gCa, gKd_{slow} and gKm. E) Average conductance composition for matched experimental cells in control (grey) and conditioned cases (blue). There is a significant increase in gKm, gCa and a decrease in gKd_{slow} (gCa p=0.015, gKm p= 0.0084, $gCaK$ p= 0.2203, gKd p= 0.2501, gKd_{slow} p=$2.01e^{-8}$, two-sided Wilcoxon signed rank test, n = 485).

current injections were assigned to the accelerating cluster, or belonged to non-adapting cells with spiking delay. The transitions between cluster types induced by the stimulation protocol are shown in Figure 5D. This figure considers only those cells in which responses both before and after conditioning could be clearly assigned to a cluster. In total, 68% of the cells (n = 50) changed their original cluster as a result of subthreshold conditioning. This quantitative result supports the observation that cells tend to transition towards more adapting and intrinsic burst profiles. 70% of cells initially belonging to the non-adapting cluster exhibited such changes in response (14 cells), with 35% moving into the intrinsic burst category, and 35% exhibiting adapting spike patterns. 5 of the 6 cells from the adapting cluster (83%) switched to the intrinsic burst type. Most of the cells for which the firing pattern did not change were already in the most common target states of transitions. For example, 89% of the intrinsic bursting cells did not change cluster. This provides further evidence for a predominantly unidirectional change of firing patterns in response to conditioning. The 7 cells that could not be consistently classified under control conditions were all correctly classified after the stimulation. They showed the same transition tendencies: 5 moved into the intrinsic bursting cluster, the other 2 became adapting.

We next aimed to infer which underlying parameters could be responsible for the systematic transitions. Our results showing that phosphorylation inhibition blocks the conditioning effect support the hypothesis that the prime candidate for this plasticity is a change in the profile of active conductances. We explored this possibility using simulations of action potential discharge in a conductance-based single compartment neuron model containing 10 voltage and calcium gated ion channels (see Methods). The densities and kinetics of these channels were derived from experimental measurements of CA3 pyramidal neurons (Hemond et al., 2008).

A database of representative ranges of maximal conductances that could plausibly explain the discharge patterns observed experimentally was generated using the single compartment model. To do this, the maximal conductances of the different channels were swept through ranges that would likely encompass the experimentally observed patterns. The spiking conductances were left constant, whereas we varied the conductances with longer time constant, which are responsible of the discharge dynamics: gCa , $gCaK$, gKm , gKd and gKd_{slow} (see Table 1 for the exact ranges). In this manner a total of 100'000 conductance profiles were generated. We obtained the discharge response to different levels

15

236 of current injection for each conductance profile, giving a total of 800'000 voltage traces with their associated maximal

237 conductance profiles. Every single experimental trace (coming from both, control and conditioned cases) was matched

238 against the collection of traces in the model database using the DTW algorithm on the instantaneous firing rate vectors

239 (see Figure 5C for an example). The best fits were then selected, allowing us to obtain an estimate of the maximal

240 conductance profile likely to be present in the experimental neuron (Figure 5C). The key to infer the parameters is thus

241 to recognize, via the DTW algorithm on the rate vectors, the subthreshold voltage envelope generated by the long-time

242 constant conductances, and not the precise spike times.

243 The diagram of Figure 5D represents the crucial conductances determining the transitions between discharge patterns

244 in firing pattern space. These are gKm, gCa and gKd_{slow}. For example, to move to the intrinsic burst cluster (yellow) a

245 characteristic enrichment in gKm and gCa is needed, which allows for the generation of the burst (given the presence

246 of basal levels of $gCaK$) and the spacing of further spikes. For the accelerating and delayed patterns (blue and purple),

247 the presence of gKd is important for a delayed onset of the spiking, and the slow inactivation of gKd_{slow} is necessary

248 for generating the continuous acceleration of the spike rate. In the case of the adapting patterns (green), the inclusion

249 of gKm is necessary for the slowing down of the action potentials after the initial discharge.

250 Figure 5E shows the average conductance content of the matched experimental traces in control and conditioned cases.

251 The shift towards adapting and intrinsic bursting behaviors after the conditioning corresponds to a significant increase

252 in gKm and gCa, and a decrease in gKd_{slow} (gCa p=0.015, gKm p= 0.0084, $gCaK$ p= 0.2203, gKd p= 0.2501, gKd_{slow}

253 p=$2.01e^{-8}$, two-sided Wilcoxon signed rank test, n = 485). This correspondence of firing patterns and biophysical

254 parameters offers an interpretation of the causes of transitions between firing behaviours induced by the conditioning.

255 Inhibition of Kv7 and calcium channels abolishes the effect of firing pattern plasticity

256 Having unraveled via the modeling study that the changes in firing pattern could correspond to an increase in gKm and

257 gCa conductances, we decided to test this prediction via pharmacological blocking of the corresponding channels. We

258 thus repeated the original experiment (Figure 1) and administrated the blockers $NiCl_2$ and $XE991$ via the perfusion

259 system after the conditioning. $NiCl_2$ is known to block T,N and L type calcium channels, with a stronger effect on the

16

260 T channel (Kochegarov, 2003), and $XE991$ is a selective blocker of the muscarinic potassium channel $Kv7/KCNQ$

261 (Brown and Randall, 2009). The results of this experiment are shown in Figure 6. Administration of the drugs blocked

262 the effect of the conditioning, with the cells loosing the change in pattern 20 min after perfusion (note that the drug took

263 3-4 min to reach the bath and start diffusing). For example, Figure 6A shows a cell that switched from accelerating to

264 intrinsic burst after conditioning. Drugs were administrated immediately after checking the conditioning effect and the

265 cell was followed for 30 min since that point (Figure 6C). 20 minutes after starting of drug perfusion the cell presented

266 an adapting burst pattern, which became adapting continuous after 30 min. The population data shows a significant

267 redistribution of spikes following drug perfusion, which goes in the opposite direction of that caused by the effect (see

268 Figures 6E and F). Note that in the absence of the drugs, we have demonstrated that the plasticity is long-lasting over

269 the course of these 30 min (Figure 3). Below each trace (Figures 6B and D), the model estimate of its conductance

270 distribution is shown, as explained in Figure 5C. An increase in gCa and gKm conductances is observed after the

271 conditioning, which then decreases after application of their corresponding channel blockers.

272 We noted that a residual adaptation remained in some neurons after the drug administration. This could likely be

273 due to the low concentration of $XE991$ employed (10 μm), although it could also be due to the small acceleration

274 at the beginning of the trace given by the delay present in these neurons. We decided to identify whether gKd was

275 responsible for such delay as hinted by the model (Figure 6D). D-type currents, caused by Kv1 channels, can be

276 blocked by low concentrations of 4-aminopyridine (4-AP). We thus repeated the experiment using 4-AP and $NiCl_2$

277 as conductance blockers (see Figure S3). After successful conditioning of the cells (see Figure S3A for an example),

278 the drugs were administered via the perfusion system. As in the previous experiment, the burst response presented

279 by the neuron, likely caused by calcium channels, was abolished. 15 min after perfusion the delay presented by the

280 neuron was also removed, with the cell adopting an adapting continuous pattern. Middle panel of Figure S3B shows

281 the effect of 4-AP in removing the delay of the population of cells. There is a significant reduction of the timing of

282 the first spike comparing to the $XE991$ experiment. For this subset of cells, no effect on the fraction of spikes was

283 found after drug perfusion (see Figure S3E and F). This is likely due to the cells keeping adaptation profiles with no

284 delay, in comparison with the previous set of experiments. Figures S3B and D show the corresponding conductance

17
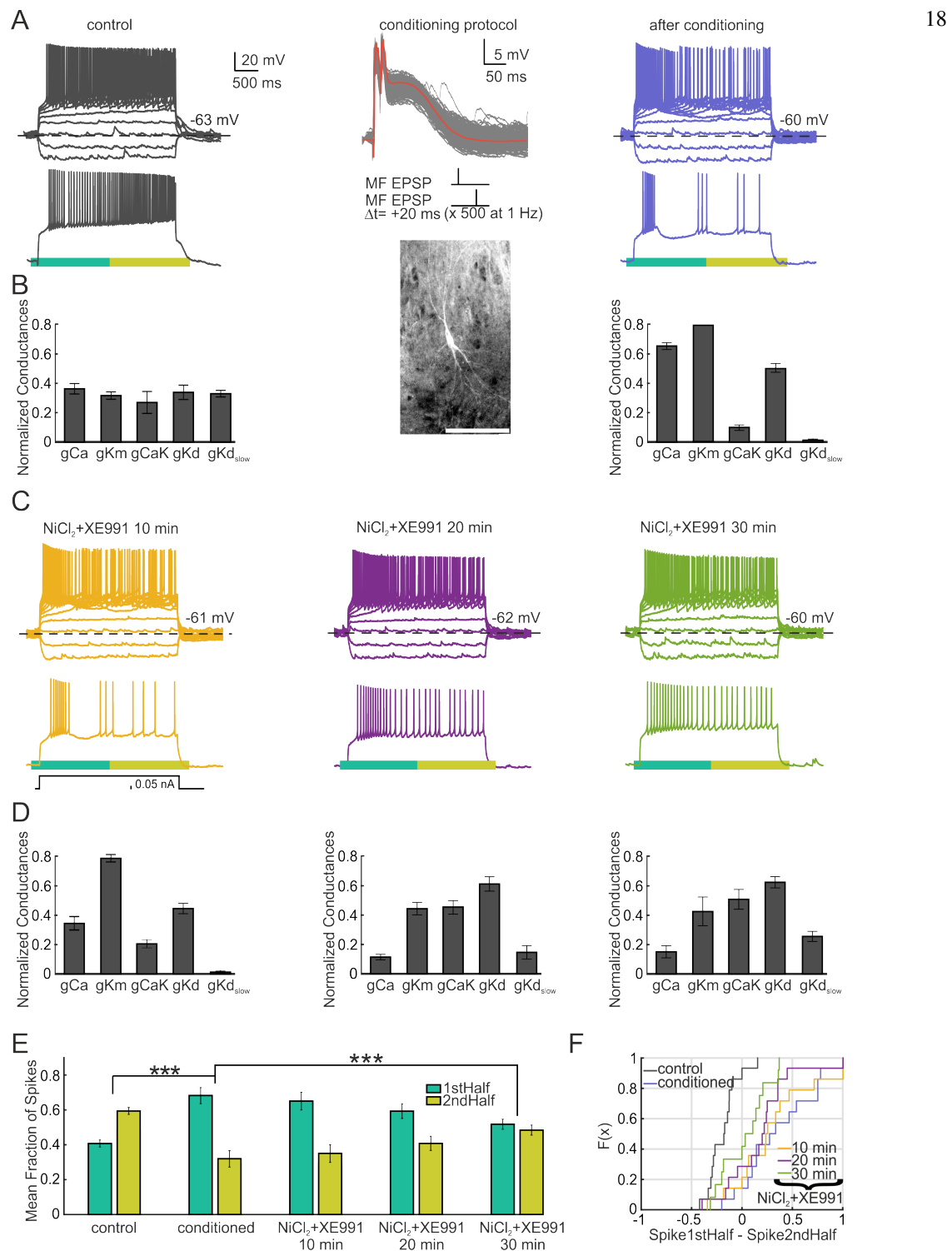
Figure 6. Inhibition of $Kv7$ and calcium channels abolish the effect of the conditioning. A) Example of a CA3 cell with accelerating pattern (grey). After conditioning via mossy fiber stimulation (protocol shown in the inset, red line shows the median.) the cell becomes intrinsic burst (blue). A biocytin staining of the cell is depicted below the protocol (scale bar = 200 μm). C) After the conditioning, $NiCl_2$ and $XE991$ were administered via the perfusion system (200 and 10 μM, respectively). The pattern was checked every 10 min since starting of perfusion. The drug took 3-4 minutes to reach the bath. 20 min since perfusion the cell presents an adapting burst pattern (purple). 10 min later the pattern can be catalogued as adapting continuous. B) and D) conductance distribution of every trace estimated via the model as done in Figure 5. Conditioning and consequent drug application affect the distribution of the conductance values. E) Mean fraction of spikes for the population in the first and second half of the voltage trace during the course of the experiment. A significant redistribution on the fraction of spikes towards the first half is observed after conditioning (n=14, p=0.0001, two-sided Wilcoxon signed rank test). This tendency is reverted during the drug application (n=14, p=7.2e-8, repeated measures ANOVA) F) Empirical cumulative distribution function for the data shown in E.

285 fits obtained from the voltage traces. The perfusion of the drugs results in a reduction of *gCa* and *gKd*, but not *gKm*

286 as in the previous set of experiments. The present data indicate that the effect of firing pattern plasticity is likely

287 being mediated by a recruitment of *gKm* and *gCa* conductances, with *gKd* necessary for shaping the delay of the spike

288 response observed in the majority of the traces.

289 **Conditioning elicits a change in firing pattern on CA3 neurons in the acute slice preparation**

290 This study was performed on organotypic cultures, derived from brain slices of newborn rats that were incubated

291 for three weeks using the roller-tube technique (Gähwiler, 1981). Organotypic cultures have been used extensively

292 to characterize electrophysiological properties of hippocampal neurons and it is known that the tissue preserves the

293 anatomical organization of the adult hippocampus, as well as its connectivity and characteristic spontaneous activity

294 (Gähwiler, 1988; Okamoto et al., 2014). However, hippocampal slices are derived from immature brains and this raises

295 the question of whether the observed transitions of firing patterns are likely to happen in the mature tissue or whether

296 they reflect activity-dependent acquisition of firing properties of neurons in the developing and more plastic brain. We

297 thus decided to test whether this type of plasticity is also present on a different preparation, acute slices derived from

298 mice between post natal days 15 and 22. Results are shown in Figure 7. Cells in the CA3 area were recorded and

299 conditioned via somatic current injection (as in Figure 4). A subset of cells were also condioned via the mossy fiber

300 pathway. In general, the conditioning elicited an increase in burstiness at the end of the voltage trace, which was higher

301 in frequency of that encountered in the organotypic case. For example, the cell in Figure 7A presented a non-adapting

302 pattern in control conditions. After conditioning the cell showed a delay burst pattern. A subset of cells also presented

303 an increase in adaptation (Figure 7B) as observed in the organotypic slice case (Figure 5D). A significant change in the

304 fraction of spikes was found at the population level (Figures 7C and D). These results indicate that conditioning elicits

305 a change in firing pattern in the acute slice preparation, suggesting the firing pattern plasticity is a generic property of

306 CA3 cells.
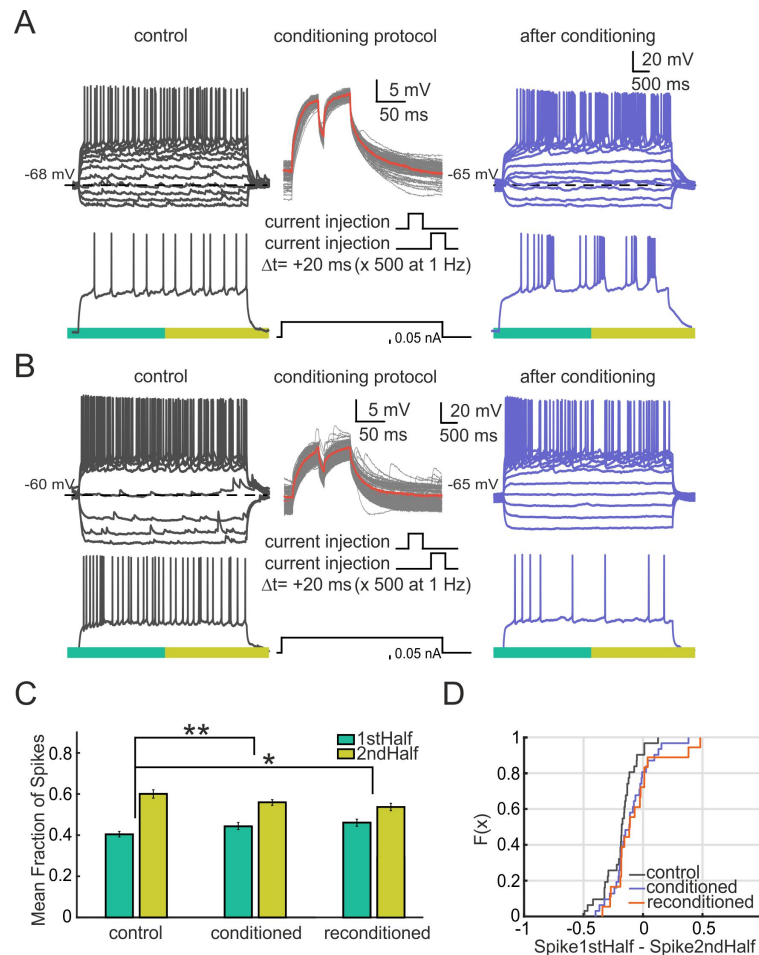
Figure 7. Conditioning changes the firing pattern of CA3 neurons in the acute slice preparation. A) Example of a cell with a non-adapting firing pattern in control conditions (grey). The cell is conditioned via somatic current injections (as in Figure 4). Protocol is shown in the inset. The firing pattern of the cell changes towards delay bursting (blue). B) Cell presenting a non-adapting burst firing pattern in control conditions. After somatic conditioning the cell presents an adapting firing response. C) Mean fraction of spikes for the population in the first and second half of the voltage trace during successive conditionings. There is a significant redistribution of the fraction of spikes after the conditioning (control-conditioned, n = 31, p=0.003, two-sided Wilcoxon signed rank test) (control-conditioned-reconditioned, n = 31, p=0.04, repeated measures ANOVA) D) Empirical cumulative distribution Function for the data shown in C. The number of spikes for the first half of the trace minus the spikes for the second half is shown for every cell.

Discussion

The diversity of firing patterns upon step current injection that neurons present have been studied and catalogued for decades (McCormick et al., 1985; Markram et al., 2004; Ascoli et al., 2008). However, why neurons have evolved these diversity of responses remains still an open issue. As a form of rapid intrinsic plasticity which operates on the spike-timing, we shown here that CA3 neurons can switch between the main established suprathreshold discharge categories (Ascoli et al., 2008) after only a few minutes of subthreshold conditioning. This effect occurred upon input delivered either to their somata by activation of their synapses, or by direct intrasomatic current injection. The effect of conditioning was long-lasting, and abolished in the presence of PKA and PKC inhibitors, indicating that phosphorylation over the few minutes of conditioning is necessary for the changes in firing pattern. Hierarchical cluster analysis showed that the transitions observed are more likely towards adapting and intrinsic burst responses. Using a conductance-based neuron model and pharmacological blocking, we found that this shift can be explained by recruitment of calcium and M-type potassium conductances. The effect of the conditioning was also observed in CA3 neurons recorded from acute slices derived from juvenile mice, suggesting that this form of plasticity is a generic property of these cells. These results indicate that, on the time scale of minutes, CA3 neurons modulate their intrinsic firing pattern depending on their history of ongoing subthreshold activity.

An intrinsic plasticity mechanism shapes the characteristic firing pattern of CA3 neurons

Neurons are plastic elements that can adjust their excitability by tuning membrane conductances in response to network activity (Turrigiano et al., 1994; Desai et al., 1999; Fan et al., 2005). This phenomena has been well characterized in the context of homeostatic plasticity (Turrigiano and Nelson, 2004). However, the time scale of those mechanisms typically extends over hours, and involves processes of gene expression (Lee et al., 2005), whereas in our experiments the changes were observed after only a few minutes of conditioning. Furthermore, we show that the effect is abolished by blocking phosphorylation, which also points towards a faster plasticity mechanism. More recent studies indicate that changes in intrinsic excitability occur on faster time scales (Aizenman and Linden, 2000; Paz et al., 2009; Mahon and Charpier, 2012; Brager and Johnston, 2007; Hyun et al., 2013). The variables considered are generally the firing rate or threshold of the cell, which are thought to facilitate synaptic hebbian learning (Titley et al., 2017). The neurons

21

332 in our study significantly adapt their spiking dynamics, adding an extra timing dimension to the previous reports (in

333 accordance to Grasselli et al. (2016) and Campanac et al. (2013)).

334 Most of the work on intrinsic plasticity require that the cell fire during the conditioning, whereas we observe that

335 the firing patterns are modulated just by subthreshold input. Golowasch et al. (1999) already demonstrated that

336 subthreshold current pulses could modulate the currents of lobster ganglion neurons, and so their discharge. However,

337 this change required hours of stimulation. Brown and Randall (2009) and Sánchez-Aguilera et al. (2014) reported that

338 subthreshold pulses or constant subthreshold depolarization increases the first ISI or reduces the overall excitability of

339 the cell a few minutes after conditioning. In line with this work, Brown and Randall (2009) also reported that transient

340 depolarizing pulses are more effective for the induction. Finally, other studies have shown that intrinsic cell properties

341 can be affected by different neuromodulators (Brager and Johnston, 2007; Graves et al., 2012; Fujisawa et al., 2005).

342 However, our changes were induced after direct subthreshold somatic conditioning, ruling out a synaptic cause.

343 The studies cited here were performed both in acute slices and in organotypic cultures. We find that the expression of

344 the conditioning differed between these two preparations. Although induction of adaptation was found both cases, the

345 bursting induction was qualitatively different, with acute neurons switching to delay burst responses (similar to Graves

346 et al. (2012)) instead of intrinsic burst ones. These discrepancies may be given by a different channel distribution and

347 kinetics, the species employed, the developmental time point or the activity levels of the two preparations (Kapoor

348 et al., 1988; Moody and Bosma, 2005; Okamoto et al., 2014). As novel neurocentric forms of plasticity are being

349 unraveled in behaving animals (Titley et al., 2017), further studies will be needed to determine whether the firing

350 pattern plasticity is also found *in vivo* and if that is the case, which effect it may elicit on the complex dynamics of

351 fully active circuits.

Mechanisms of firing pattern transitions

353 Our modeling and pharmacological study suggests that the conductances supporting transitions through the firing

354 pattern space of CA3 cells are gKd, gKm and gCa (coupled with $gCaK$). These candidates have previously been

355 reported to shape the spiking response of hippocampal cells via activity dependent mechanisms. For example, $gCaT$

22

356 is strongly associated with the switch to bursting mode upon status epilepticus (Kim et al., 2001; Su et al., 2002),

357 while gKd is modulated by activity and influence the delay firing of the cell (Cudmore et al., 2010; Hyun et al.,

358 2013; Saviane et al., 2003). Modulation of the M-type current upon activity has also been shown in CA1 (Wu et al.,

359 2008) and in CA3 (Brown and Randall, 2009). Furthermore, rapid up- or down-regulation of ion channel maximal

360 conductances via phosphorylation or vesicle modulation due to calcium signaling has been demonstrated extensively

361 (Flavell and Greenberg, 2008; Davis et al., 2001; Zhang and Linden, 2003) and it has also been shown that the channels

362 possess a complex of scaffold proteins containing protein kinases that could selectively regulate their conductance

363 through phosphorylation (Davis et al., 2001). The exact rules that link the subthreshold input to the recruitment of

364 the different conductances remain to be elucidated, but could likely depend on calcium dynamics and possibly the

365 activation properties of the involved channels (Turrigiano and Nelson, 2004; Stemmler and Koch, 1999; Li et al.,

366 2016).

367 One of the typical transitions that we observe is the switch towards bursting behaviors. We emphasize that this is

368 not the only transition induced, but rather that special attention should be given to this bursting mechanism. It is

369 known that some neurons present this dual behavior. For example, relay cells on the thalamus become bursty upon

370 hyperpolarization because of T-type conductance inactivation (Sherman, 2001). In our case, the cells depolarized 5

371 mV in average, while kinase inhibitors blocked the effect, ruling out this hyperpolarizing cause.

372 **Functional implications of firing pattern modulation**

373 Similar firing patterns are found in multiple species within the animal phyla (McCormick et al., 1985; Turrigiano

374 et al., 1994; Yao and Wu, 2001), suggesting that they have a fundamental role in network computation. Shin et

375 al. (1999) proposed that neurons that can dynamically adapt their output firing in response to their input statistics

376 would have important advantages. By adjusting its threshold and dynamic range upon activity, a neuron could respond

377 to stimuli over a broad range of amplitudes and frequencies without compromising sensitivity, maximizing the mutual

378 information between its input and output discharge (Stemmler and Koch, 1999). Spike frequency accommodation has

379 the characteristics of a high-pass filter (Benda and Herz, 2003). Since our conditioning stimuli occurred at constant

frequencies, cells may have recruited a specific set of conductances that shift their integration properties to gain sensitivity in the new frequency range. Differences in filtering properties of brain stem neurons have also been shown to facilitate the extraction of spatial information from natural sounds (Remme et al., 2014) and most of the conductances that we identify in this study have reported to be frequency resonance candidates (Hutcheon and Yarom, 2000; Hu et al., 2002; Schreiber et al., 2004). These resonance properties of cells may also have important functional implications for neural activity and brain rhythms (Llinás, 1988; Buzsáki and Draguhn, 2004). When adjusting their discharge to more adapting patterns neurons may be changing mode from integrator to a coincidence detector (Prescott et al., 2008), helping not only to detect synchrony but also to transmit it to the network (Cudmore et al., 2010). Additionally, this fast plasticity of the firings may also be important for specific memory acquisition on the hippocampus (Kumaran et al., 2016; Benna and Fusi, 2016). CA3 is thought to be the generator of sharp wave ripples (SPW-R), a state where neurons cooperatively switch to presumably transfer memories to cortex (Buzsáki, 2015; Kumaran et al., 2016; Hunt et al., 2018). The stimulation protocol -resembling a SPW-R- may have push CA3 neurons to move to a different network state, similarly to Fujisawa et al. (2005), by possibly sensing the inputs and changing their spiking properties based on intrinsic plasticity rules (Srikanth and Narayanan, 2015).

Further studies will be needed in order to unravel the role that such firing pattern transitions may have for computations in neural circuits. A first step towards this goal must be to explore more generally how the form and frequency spectrum of somatic input signals on the long time scale affect the distinct firing patterns that neurons exhibit on the short scale. It appears that, after decades of study and cataloguing these patterns, the mystery is not whether they conform to classes or to a continuum but rather, what internal rules and computational advantages are that result neurons to converge onto these different discharge states.

Grants

Disclosures

The authors declare no competing financial interests.

Author Contributions

Conceptualization, S.S, F.B. and R.D.; Methodology, S.S. and F.B.; Software, S.S. and S.H.; Validation, S.S. and F.B.; Formal Analysis, S.S. and M.F.; Investigation, S.S., F.B. and S.H.; Resources, U.G. and K.A.C.M.; Data Curation, S.S.; Writing-Original Draft, S.S., M.F and R.D.; Visualization, F.B. and S.S.; Supervision, R.D. and M.F.; Project Administration, R.D.; Funding Acquisition, K.A.C.M., U.G. and S.S.

Acknowledgements

Materials and Methods

All experiments were conducted in accordance with the guidelines and regulations of the Cantonal Veterinary Office of Zurich; License Nr 81/2014, 89/2013, 70/2016 and 156/2017.

Electrophysiological Recordings

Rat hippocampal organotypic cultures (Gähwiler, 1981) of average postnatal age 21 days were transferred to a recording chamber and mounted on an upright microscope (Axioskop FS1; Zeiss). The cultures were superfused with an external solution (pH 7.4) containing (in mM) 148.8 Na^+, 2.7 K^+, 149.2 Cl^-, 2.8 Ca^{2+}, 2.0 Mg^{2+}, 11.6 HCO_3^-, 0.4 $H_2PO_4^-$, 5.6 D-glucose, and 10 mg/l Phenol Red. All experiments were performed at $34\,°C$. Whole-cell recordings of CA3 neurons were obtained with patch pipettes (4-7 $M\Omega$). Pipettes were filled (in mM) with 126 K-gluconate, 4 $NaCl$, 1 $MgSO_4$, 0.1 $BAPTA-free$, 0.05 $BAPTA-Ca^{2+}$, 15 glucose, 3 ATP, 5 $HEPES$ (pH was adjusted to 7.2 with

25

425 KOH) 0.1 GTP, and 10.4 byocitin. For acute experiments, 300 μm sagital hippocampal slices were prepared from

426 mice ranging 15 to 22 days old. After decapitation under isoflurane anesthesia, the brain was removed and placed in

427 oxygenated (95% O_2, 5% CO_2) and ice-cold high-sucrose artificial cerebrospinal fluid (ACSF) (pH 7.4) containing (in

428 mM) 75 sucrose, 87 $NaCl$, 2.5 KCl, 7 $MgSO_4$, 0.5 $CaCl_2$ 26 $NaHCO_3$, 1 NaH_2PO_4, and 10 D-glucose. Slices were cut

429 in this solution and then transferred for recovery to oxigenated ACSF ($pH7.4$) at 37 °C containing (in mM) 119 $NaCl$,

430 2.5 KCl, 1.3 $MgSO_4$, 2.5 $CaCl_2$ 26 $NaHCO_3$, 1.25 NaH_2PO_4, and 10 D-glucose. After 30 min of recovery, slices

431 were kept at room temperature for 1 hour before recording. During recording, slices were superfused with oxigenated

432 ACSF.

433 The recording pipettes were manually positioned under microscope control. Recorded neurons were located mostly in

434 the pyramidal cell layer. Electrophysiology and subsequent histology in a subset of the cells recorded suggest that the

435 neurons described below include mostly pyramidal cells but also a subset of smooth cells.

436 Current-voltage relationships were determined by step command potentials and had duration of 1 second to ensure

437 steady-state responses. Data were recorded using an Axopatch 200B amplifier (Molecular Devices). Series resistance

438 was monitored regularly, and was typically between 5 and 15 $M\Omega$. Cells were excluded from further analysis if this

439 value changed by more than 20% during the recording. Junction potential and bridge was not corrected.

440 Mossy fibers were stimulated with a bipolar tungsten electrode. The intensity of the stimulus was constantly adjusted

441 to evoke subthreshold post-synaptic potential responses of 15 mV on average in the recorded neuron.

442 Action potential discharges were evoked by injected current steps (-0.08 up to 1.8 nA; step increment 0.05 - 0.15 nA,

443 depending on the input resistance of the recorded cell) each lasting from 3 to 5 seconds. After this control, the neurons

444 were conditioned by mossy fibers activation, consisting of a double pulse (0.1 ms duration pulses, interval 10 - 20 ms)

445 at a frequency of 1 Hz, repeated 500 times. Thus, the conditioning period was approximately 8 minutes. In a subset of

446 experiments an interval of 60 ms was used. Immediately after this conditioning, the firing pattern of the neuron was

447 assessed again using the same step protocol. The firing pattern of these cells was assessed every 10 minutes until 40

448 minutes of recording were completed to assess long-term effects of the plasticity. In a another subset of experiments,

mossy fiber subthreshold responses were mimicked by injecting somatically and at a frequency of 1 Hz double step current pulses of 50 ms of duration and 20 ms of interstep interval. The amplitude of the pulse was adjusted in order to get a depolarization of 15 mV on average.

For any set of experiments, 1 cell per slice was recorded and 6 slices per rat on average (of either sex) were used for preparation of the organotypic cultures. A minimum of 8 cells were used for each set of experiments.

Pharmacology

All drugs were applied to the slices via the perfusion system. Calcium currents were blocked by applying $NiCl_2$ at 200 μM. D-type currents (Kv1 channels) were blocked by application of low concentrations (30 μM) of 4-aminopyridine ($4-AP$). The M-current was blocked by application of $XE991$ at 10 μM, which targets $Kv7/KCNQ$ channels (Brown and Randall, 2009). $4-AP$, $NiCl_2$ and $XE991$ were purchased from Sigma-Aldrich (A78403, 339350, X2254). Times indicated in the figures reffer to the time elapsed since starting of the drug perfusion. The timing for the drug to reach the bath was estimated of 3-4 minutes.

Histology

Hippocampal slice cultures were prepared for morphological assessment by fixing in freshly prepared 4% paraformaldehyde in 0.1 M phosphate buffer (PB) at pH 7.4 overnight at 4 °C; washing three times in phosphate-buffered saline (PBS, 1.5 mM KH_2PO_4, 8.5 mM Na_2HPO_4, 137 mM $NaCl$, and 3 mM KCl, pH 7.4); and permeabilizing at room temperature in PBS that contained 10% heat-inactivated donkey serum, and 1% Triton X-100. Then they were incubated overnight at 4 °C with streptavidin conjugated with Alexa (546λ). The cultures were washed again three times in PBS, and then mounted in Fluorostab (Bio-Science Products AG, Emmenbrucke, Switzerland) and coverslipped. High-resolution images were obtained using laser scanning confocal microscopy (Leica TCS SP2, Leica Microsystems, Heidelberg, Germany).

Data analysis

Signals were digitized at 10 kHz and analysed off-line using pCLAMP 10 (Molecular Devices) and Matlab (MathWorks). Analysis of the voltage traces was performed similar to Chen et al. (2015). The average resting membrane potential of each neuron was estimated as the mean membrane potential during the first 100 ms of current-injection protocol (before injection of the step-current pulses). Input resistance was obtained by measuring the voltage drop across the hyperpolarizing trace of the step-current pulses. APs were located using median filtering, and the threshold was inferred as the point at which the derivative of the voltage trace exceeded 5 mV/ms. AP amplitude was measured from threshold-to-peak and AP afterhyperpolarization (AHP) from the threshold to through. Half-width was estimated as the full width at half-maximal amplitude. The fraction of spikes of a cell at a given time was computed by calculating the mean of the fraction of spikes of the individual current injections. At the population level the mean of this quantity was calculated.

Data was tested for normality using a one-sample Kolmogorov-Smirnov test. A paired t-test was used for statistical comparisons between conditions with normally distributed data and a two-sided Wilcoxon signed rank test was used otherwise. The exact p-values of the tests and the sample number for each experiment are indicated on the figure legends in the results section. A clustering analysis was also performed for the synaptic conditioning group, and it is described on the following section. All the statistical analysis were performed using Matlab (MathWorks).

Cluster analysis of discharge traces

The firing patterns of the neurons were categorized by hierarchical clustering of their discharge patterns. The dataset consisted of all voltage traces recorded from neurons in response to step-wise current injections with different amplitudes, including recordings before and after conditioning. For any one neuron, the collection of responses to different current injections represents the signature of the electrical type. However, for inherent verification of our cluster procedure, we chose to treat each response independently. In this way successful clustering could be confirmed by its ability to assign responses from the same neuron into the same category.

The clustering measured similarity of a feature vector derived from the voltage traces. First the recorded voltage traces

28

were converted into a time series of the instantaneous firing rates. The instantaneous firing rate at each spike was taken as 1/Inter-spike-Interval (ISI). Then the instantaneous rates where linearly interpolated across the spike times at 1 ms time intervals over 6 seconds (5 second current injection step, plus 1 second on and offset), and normalized by the maximum firing rate. Finally, a characteristic feature vector of a common length of 600 elements was obtained by down-sampling the interpolated rate traces by a factor of 10, in order to make them computationally tractable to the similarity measurement.

Similarity distances between pairs of traces were calculated using the Dynamic Time Warping (DTW) measure (Berndt and Clifford, 1994). DTW takes into account that two similar signals can be out of phase temporally, and aligns them in a non-linear manner through dynamic programming (Keogh and Ratanamahatana, 2005). The algorithm takes two time series $Q = \langle q_1, q_2, \ldots, q_n \rangle$ and $C = \langle c_1, c_2, \ldots, c_m \rangle$ and computes the best match between the sequences by finding the path of indices that minimizes the total cumulative distance

$$\mathrm{DTW}(Q,C) = \min \sum_{k=1}^{K} w_k \tag{1}$$

where w_k is the cost of alignment associated with the kth element of a warping path W. A warping path starts at q_1 and c_1 respectively, and finds a monotonically increasing sequence of indices i^k and j^k, such that all elements q_i in Q and c_j in C are visited at least once, and for the final step of the path $i^{end} = n$ and $j^{end} = m$ holds. The optimal DTW distance is the cumulative distances $y(i, j)$, corresponding to the costs of the optimal warping path $\langle q_1, \ldots, q_i \rangle$ and $\langle c_1, \ldots, c_j \rangle$. This distance can be computed iteratively by dynamic programming:

$$y(i, j) = d(q_i, c_j) + \min\{y(i-1, j-1), y(i-1, j), y(i, j-1)\} \tag{2}$$

where $d(q_i, c_j)$ is the absolute difference between the elements of the sequence. The optimal warping path is obtained by backtracking from the final element $y(n, m)$, and finding which of the three options (increasing i only, increasing j only, or increasing i and j simultaneously) led to the optimal warping distance, until $i = 1, j = 1$ is reached. A warping

29

513   window constraint of 10% of the vector size was chosen (Keogh and Ratanamahatana, 2005).

514   The pairwise DTW distances were used to perform hierarchical clustering by Ward's algorithm (Ward Jr, 1963). The

515   number of classes increases with the level of the hierarchy. We choose to cut the tree at a level that provided sufficient

516   structure to interpret the hierarchy in terms of recognized response types (Ascoli et al., 2008).

517   Every recording for a given cell was treated as an independent observation, and could in principle be assigned to any

518   cluster. If the electrophysiological state of the cell is expressed in all of its responses, then we expect that all the

519   independent observations derived from that cell should be assigned to the same cluster. However, traces derived from

520   current injections to the same cell in different conditions (pre- or post-stimulation) are expected to be assigned to

521   different clusters if there is significant change in the underlying electrophysiological state.

522   In fact the independent traces did not cluster perfectly. Instead, the majority of independent observations derived

523   from a given state clustered together and there were a few that fell into other clusters. Therefore, we chose to label

524   the electrical type of each cell according to the cluster that contained the mode of the traces for one set of current

525   injections. Cells for which no clear dominant cluster could be identified, e.g. because half of the traces fell into one

526   cluster, and half of them into another, were labeled as unclassified. A cluster transition was recognized whenever the

527   cell was assigned to different clusters before and after the stimulation protocol.

528   The analysis was performed using custom-written software in MatlabR2011b. The implementation of the DTW

529   algorithm was obtained from Matlab Central `http://www.mathworks.com/matlabcentral/fileexchange/`

530   `43156-dynamic-time-warping-dtw`.

Neuron simulation model

532   A single cylindrical compartment, conductance-based neuronal model was used for all simulations. The length and

533   diameter of the cylinder are set at equal dimensions to avoid spatial discretization problems in a single compartment

534   (Cooley and Dodge, 1966; De Schutter and Bower, 1994). The passive properties associated with the model were

535   obtained from Hemond et al. (2008). We set the length and diameter of our compartment to 50 μm. The active

536 properties were modeled by including appropriate voltage and calcium gated ion channels whose density and kinetics

537 were obtained from experimental recordings performed in CA3 neurons (Hemond et al., 2008). All the conductances

538 included in the model where obtained from this work, except for gKd_{slow}, which had to be added in order to match the

539 accelerating traces. We found that a 10 fold increase in the time constant of inactivation of gKd significantly improved

540 the accelerating index. A similar slow gKd current matching these kinetics has actually been found in CA3 neurons

541 (Luthi et al., 1996). The faster Kd current, has been previously reported both in cortex and hippocampus (Storm, 1988;

542 Cudmore et al., 2010; Hyun et al., 2013; Miller et al., 2008). Throughout the manuscript, we refer to the channels

543 as conductances. The simulations were performed using NEURON (Hines and Carnevale, 1997). We choose an

544 integration step of 25 μs, which was approximately 1% of the shortest time constant in the model. The voltage- and

545 time-dependent currents followed the Hodgkin and Huxley formalism (1952):

$$C \cdot \frac{\mathrm{d}V}{\mathrm{d}t} = -(I_{Na} + I_{Kdr} + I_{Kd} + I_{KA} + I_{Km} + I_{CaK} + I_{CaL} + I_{CaT} + I_{CaN} + I_{Leak}) \tag{3}$$

546 Each current I_x is described by the equation

$$I_{(v,t)} = \bar{g} \cdot m \cdot h \cdot (V_{(t)} - E) \tag{4}$$

547 where $\bar{g}$ is the maximal conductance, m and h are activation and inactivation terms, V is the membrane potential, and

548 E the reversal potential of the channel. The reversal potentials for Na^+ and K^+ were E_{Na} = 50 mV and E_K = -85

549 mV, respectively. The equations describing the different channel kinetics (m, h) for every current were obtained from

550 Hemond et al. (2008). Following this reference, the three calcium conductances (T, N and L) were incorporated into

551 a single parameter gCa.

552 The intracellular calcium dynamics were modeled as originally described by Hemond et al. (2008):

553

$$\frac{\mathrm{d}[Ca^{2+}]_i}{\mathrm{d}t} = \frac{\mathrm{I}_{Ca}}{2Fv} - \frac{[Ca^{2+}]_i - 0.0001}{\tau_{Ca}} \tag{5}$$

554 The first term of the above equation describes the change caused by Ca^{2+} influx into a compartment with volume v. F

555 is the Faraday constant, I_{Ca} is the calcium current and τ_{Ca} is the time constant of Ca^{2+} diffusion.

556 The occasional decrease in spike amplitude seen in some of the experimental traces is probably due to sodium

557 inactivation. We choose not to include this feature in the model, because it does not affect the overall dynamics

558 of the spike discharge itself.

559 The model is available online at ModelDB `https://senselab.med.yale.edu/ModelDB/enterCode.`

560 `cshtml?model=228599`

Model Database of Traces

561

562 In order to get a conductance estimate for every voltage trace, we used the DTW algorithm to find the best fit to a

563 database of voltage traces generated by the model. We varied the maximal conductances of our model into ranges

564 that would contain our observed set of experimental voltage traces. The spiking conductances were left constant and

565 gCa , $gCaK$, gKm , gKd and gKd_{slow} were varied. The search of a valid conductance space was done manually,

566 with the starting values provided by the report of Hemond et al. (2008) to reproduce CA3 firings. For the values

567 and ranges used to generate the database see Table 1. A total of 100'000 conductance vectors were generated by

568 combining the different conductances. The firing pattern of every conductance vector was produced at 8 different

569 levels of step-current injection, obtaining a total of 800'000 voltage traces. An integration step of 0.2 ms was used.

570 After generating the database non-spiking traces were removed, together with traces with saturating spikes. This

571 led to a total of 73'024 voltage traces composing the conductance database. Every experimental trace, for both the

572 control and conditioned case, was compared pairwise using the DTW algorithm with the set of voltage traces from

573 the database. The 10 best fits were then selected in order to have an estimate of the conductance composition of the

574 experimental trace.

32

| Conductances and Current	Employed ranges
g_{Na}	0.04
g_{Kdr}	0.01
g_{Ka}	0.05
g_{Ca}	$1e^{-6} + (0 : 1e^{-4} : 9e^{-4})$
g_{CaK}	$1e^{-6} + (0 : 1e^{-4} : 9e^{-4})$
g_{Km}	$1e^{-6} + (0 : 1e^{-4} : 9e^{-4})$
g_{Kd}	$1e^{-6} + (0 : 1e^{-4} : 9e^{-4})$
$g_{Kd_{slow}}$	$1e^{-6} + (0 : 1e^{-4} : 9^{e}-4)$
I	$0.2 : 0.16 : 1.32$
Total conductance vectors	100'000
Total traces	800'000

Table 1. Range of maximal conductance values used to generate the model database of voltage traces. A model database of voltage traces, which includes all the observed experimental firing patterns, was generated by varying 5 maximal conductances (gCa , $gCaK$, gKm , gKd and gKd_{slow}) over a given range. Different ranges of step current I were also needed to reveal the different firing types. A total of 100'000 conductance vectors were generated by combining the different conductances. The firing pattern of every conductance vector was produced at several levels of step-current injection, obtaining a total of 800'000 voltage traces. Note that $gCaT$, $gCaN$ and $gCaL$ are englobed under the single parameter gCa.

575 The firing pattern of the model traces was simulated using 1 second of step current duration. Note that this differs from

576 the time scale of our experimental traces, which were unraveled at 3-5 seconds of step current. Although generation

577 of the traces for this longer duration was possible, the resulting firing patterns did not reproduce faithfully all the

578 spiking dynamics encountered in the experiments. A change in channel kinetics (Hemond et al., 2008), an additional

579 conductance, or a dendritic load could possibly solve the issue. The objective however was to gain an intuition on the

580 possible conductance distribution changes induced by the conditioning. This together with computational reasons to

581 generate the database led us to proceed with the simulations using a 1 second current step.

582 **Supplementary Material**
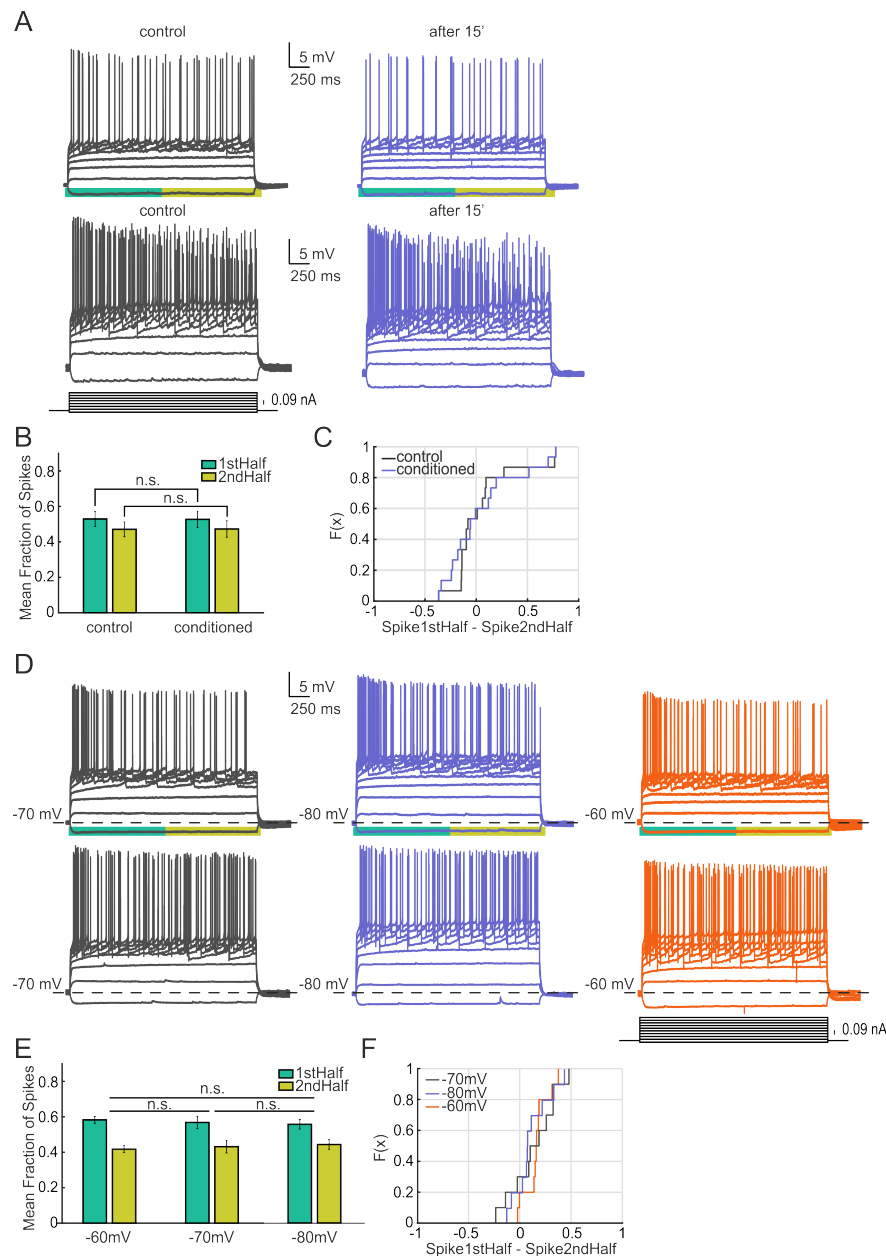
Figure S1. CA3 firing patterns are stable over time as well as to changes in resting membrane potential. Firing pattern transitions are not elicited by step current injection alone. A) Examples of two cells whose firing pattern have been measured by step-wise current injection (protocol showed in the inset). The cells do not show changes in firing pattern after 15 min of recording. B) Mean fraction of spikes for the population in the first and second half of the voltage trace for both control and conditioned cases. No significant redistribution on the fraction of spikes is observed (n = 15, p=0.583, two-sided Wilcoxon signed rank test). C) Empirical cumulative distribution Function for the data shown in B. Every individual case is represented as the number of spikes for the first half of the trace minus the spikes for the second half. D) Firing pattern transitions are not elicited by sustained shifts in membrane potential. Examples of two cells that have been hold at different membrane potentials through steady current injection (-70, -80 and -60 approximately). After changing the holding potential of the recorded neuron the firing pattern was measured by step-wise current injection (protocol showed in the inset). No transitions of firing pattern were observed at any of the different holding potentials. E) Mean fraction of spikes for the population in the first and second half of the voltage trace for every condition. No significant redistribution on the fraction of spikes is observed (Vm 60 vs 70, p=0.652; Vm 60 vs 80, p=0.084; Vm 70 vs 80, p=0.695) (n = 10, two-sided Wilcoxon signed rank test)). F) Empirical cumulative distribution function for the data shown in E. Every individual case is represented as the number of spikes for the first half of the trace minus the spikes for the second half.
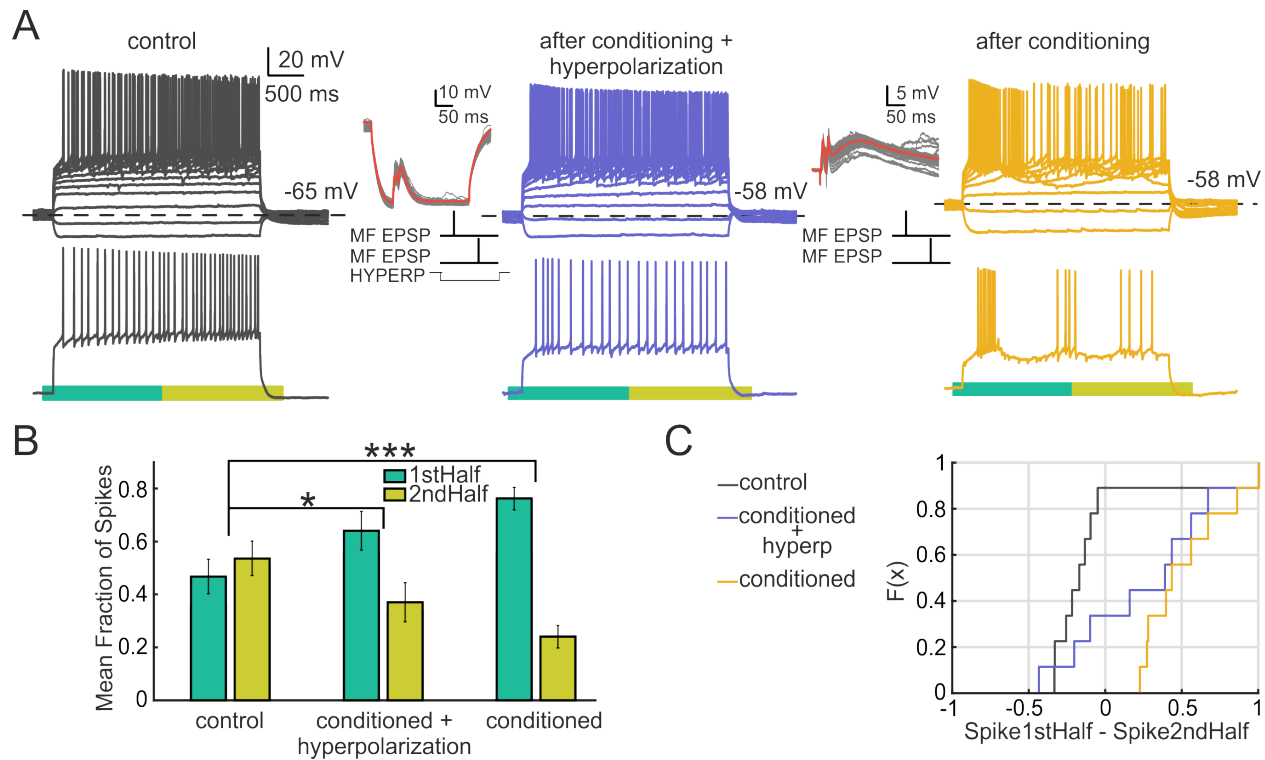
Figure S2. The effect of mossy fiber conditioning does not require somatic depolarization. Conditioning was performed while hyperpolarizing the cell with a negative current pulse. A) Cell that presents an accelerating pattern in control conditions (grey). Conditioning (MF double pulse, delta 20 ms given at 1 Hz) was elicited under the presence of an hyperpolarizing current step (protocol is shown in the inset, red line indicates the median). The cell changes its firing pattern to an non-adapting burst response. Thereafter, the cell is reconditioned via only the mossy fiber double pulse. After this conditioning the cell presents an intrinsic burst pattern. B) Mean fraction of spikes for the population in the first and second half of the voltage trace during the successive conditionings. A significant redistribution on the fraction of spikes is observed after the conditioning under the hyperpolarizing pulse (n=9, p=0.016, two-sided Wilcoxon signed rank test). After a second conditioning, without hyperpolarization, a stronger effect is found (n=9, p=0.008, two-sided Wilcoxon signed rank test). C) Empirical cumulative distribution Function for the data shown in B. The number of spikes for the first half of the trace minus the spikes for the second half is shown for every cell (n=9).
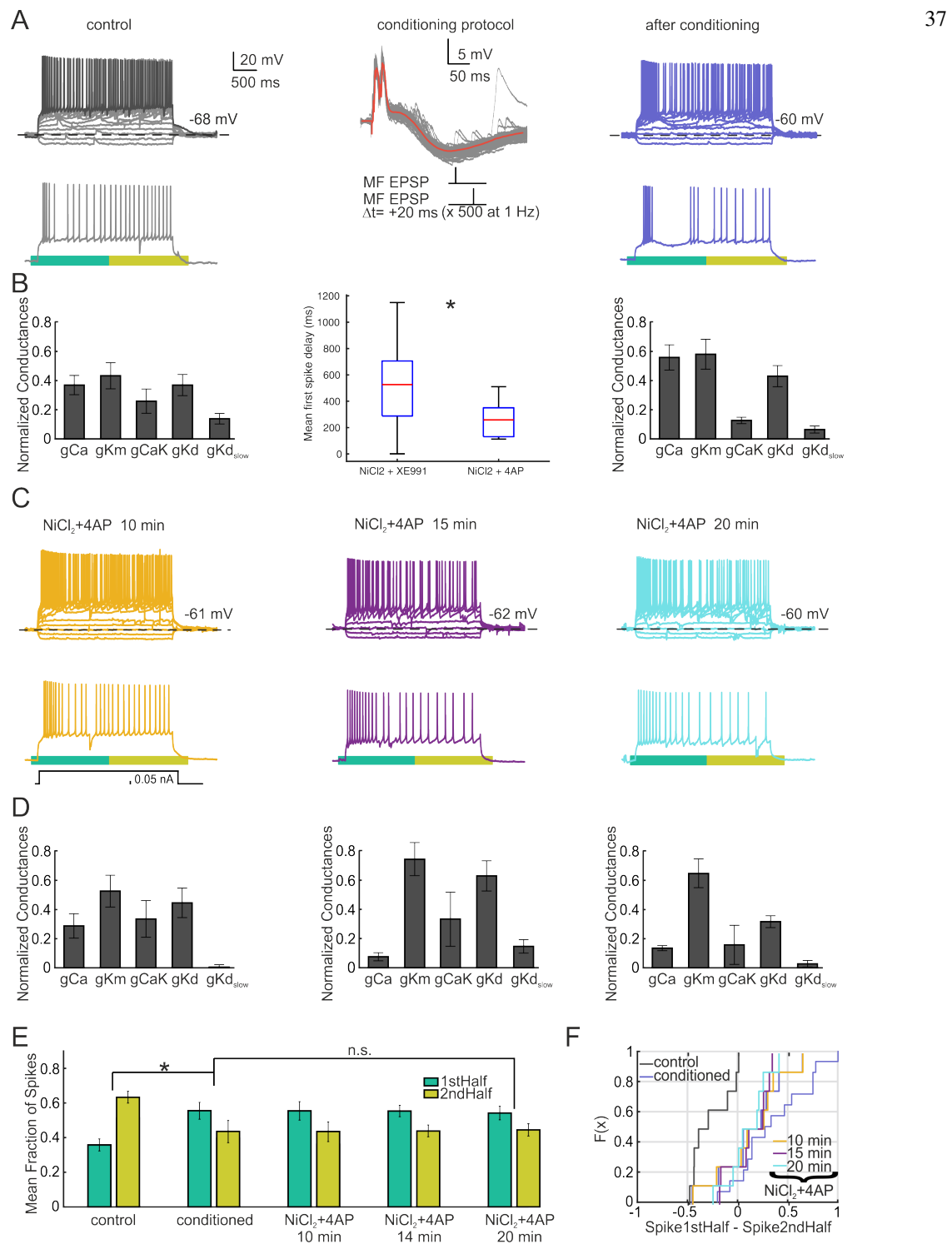
Figure S3. Inhibition of $Kv1$ and calcium channels reduces the delay of the traces but does not abolish the effect on the fraction of spikes. A) Cell with an adapting burst firing pattern in control conditions (grey) that switches to intrinsic burst after conditioning (blue). C) After 15 min of bath application of 4-AP and $NiCl_2$ (at 30 and 200 μM) the cell switches to an adapting continuous pattern, with no delay (purple and blue traces). B) and D) Conductance model fits for every voltage trace. The middle panel shows the mean delay for the first spike when 4-AP is administrated with $NiCl_2$ via the perfusion system, in comparison with XE991. A decrease on this delay by 4-AP is observed (n=8, p=0.02, two-sided Wilcoxon signed rank test). E) Mean fraction of spikes for the population in the first and second half of the voltage trace during the experiment. A significant redistribution on the fraction of spikes in favor of the first half is observed after conditioning (n=8, p=0.015, two-sided Wilcoxon signed rank test). Application of the drugs did not have an effect on the fraction of spikes (n = 8, p=0.98, repeated measures ANOVA) C) Empirical cumulative distribution function for the data shown in E.

Bibliography

Aizenman CD, Linden DJ (2000) Rapid, synaptically driven increases in the intrinsic excitability of cerebellar deep nuclear neurons. *Nature neuroscience* 3:109–111.

Ascoli GA, Alonso-Nanclares L, Anderson SA, Barrionuevo G, Benavides-Piccione R, Burkhalter A, Buzsáki G, Cauli B, DeFelipe J, Fairén A et al. (2008) Petilla terminology: nomenclature of features of gabaergic interneurons of the cerebral cortex. *Nature Reviews Neuroscience* 9:557–568.

Belmeguenai A, Hosy E, Bengtsson F, Pedroarena CM, Piochon C, Teuling E, He Q, Ohtsuki G, De Jeu MT, Elgersma Y et al. (2010) Intrinsic plasticity complements long-term potentiation in parallel fiber input gain control in cerebellar purkinje cells. *Journal of Neuroscience* 30:13630–13643.

Benda J, Herz AV (2003) A universal model for spike-frequency adaptation. *Neural computation* 15:2523–2564.

Benna MK, Fusi S (2016) Computational principles of synaptic memory consolidation. *Nature neuroscience* .

Berndt DJ, Clifford J (1994) Using dynamic time warping to find patterns in time series. In *KDD workshop*, Vol. 10, pp. 359–370. Seattle, WA.

Brager DH, Johnston D (2007) Plasticity of intrinsic excitability during long-term depression is mediated through mglur-dependent changes in ih in hippocampal ca1 pyramidal neurons. *Journal of Neuroscience* 27:13926–13937.

Brandalise F, Carta S, Helmchen F, Lisman J, Gerber U (2016) Dendritic nmda spikes are necessary for timing-dependent associative ltp in ca3 pyramidal cells. *Nature Communications* 7:13480.

Brandalise F, Gerber U (2014) Mossy fiber-evoked subthreshold responses induce timing-dependent plasticity at hippocampal ca3 recurrent synapses. *Proceedings of the National Academy of Sciences* 111:4303–4308.

Brown JT, Randall AD (2009) Activity-dependent depression of the spike after-depolarization generates long-lasting intrinsic plasticity in hippocampal ca3 pyramidal neurons. *The Journal of physiology* 587:1265–1281.

Butt SJ, Fuccillo M, Nery S, Noctor S, Kriegstein A, Corbin JG, Fishell G (2005) The temporal and spatial origins of cortical interneurons predict their physiological subtype. *Neuron* 48:591–604.

607 Buzsáki G (2015) Hippocampal sharp wave-ripple: A cognitive biomarker for episodic memory and planning.
608 *Hippocampus* 25:1073–1188.

609 Buzsáki G, Draguhn A (2004) Neuronal oscillations in cortical networks. *Science* 304:1926–1929.

610 Campanac E, Gasselin C, Baude A, Rama S, Ankri N, Debanne D (2013) Enhanced intrinsic excitability in basket
611 cells maintains excitatory-inhibitory balance in hippocampal circuits. *Neuron* 77:712–722.

612 Cauli B, Porter JT, Tsuzuki K, Lambolez B, Rossier J, Quenet B, Audinat E (2000) Classification of
613 fusiform neocortical interneurons based on unsupervised clustering. *Proceedings of the National Academy of*
614 *Sciences* 97:6144–6149.

615 Cohen S, Greenberg ME (2008) Communication between the synapse and the nucleus in neuronal development,
616 plasticity, and disease. *Annual review of cell and developmental biology* 24:183–209.

617 Connors BW, Gutnick MJ (1990) Intrinsic firing patterns of diverse neocortical neurons. *Trends in*
618 *neurosciences* 13:99–104.

619 Cooley J, Dodge F (1966) Digital computer solutions for excitation and propagation of the nerve impulse. *Biophysical*
620 *journal* 6:583–599.

621 Cudmore RH, Fronzaroli-Molinieres L, Giraud P, Debanne D (2010) Spike-time precision and network synchrony are
622 controlled by the homeostatic regulation of the d-type potassium current. *Journal of Neuroscience* 30:12885–12895.

623 Davis MJ, Wu X, Nurkiewicz TR, Kawasaki J, Gui P, Hill MA, Wilson E (2001) Regulation of ion channels by protein
624 tyrosine phosphorylation. *American Journal of Physiology-Heart and Circulatory Physiology* 281:H1835–H1862.

625 De Schutter E, Bower JM (1994) An active membrane model of the cerebellar purkinje cell. i. simulation of current
626 clamps in slice. *Journal of neurophysiology* 71:375–400.

627 Debanne D, Inglebert Y, Russier M (2019) Plasticity of intrinsic neuronal excitability. *Current opinion in*
628 *neurobiology* 54:73–82.

Dehorter N, Ciceri G, Bartolini G, Lim L, del Pino I, Marín O (2015) Tuning of fast-spiking interneuron properties by an activity-dependent transcriptional switch. *Science* 349:1216–1220.

Desai NS, Rutherford LC, Turrigiano GG (1999) Plasticity in the intrinsic excitability of cortical pyramidal neurons. *Nature neuroscience* 2:515–520.

Druckmann S, Hill S, Schürmann F, Markram H, Segev I (2013) A hierarchical structure of cortical interneuron electrical diversity revealed by automated statistical analysis. *Cerebral Cortex* 23:2994–3006.

Dumitriu D, Cossart R, Huang J, Yuste R (2007) Correlation between axonal morphologies and synaptic input kinetics of interneurons from mouse visual cortex. *Cerebral cortex* 17:81–91.

Fan Y, Fricker D, Brager DH, Chen X, Lu HC, Chitwood RA, Johnston D (2005) Activity-dependent decrease of excitability in rat hippocampal neurons through increases in ih. *Nature neuroscience* 8:1542–1551.

Flavell SW, Greenberg ME (2008) Signaling mechanisms linking neuronal activity to gene expression and plasticity of the nervous system. *Annual review of neuroscience* 31:563.

Fujisawa S, Matsuki N, Ikegaya Y (2005) Single neurons can induce phase transitions of cortical recurrent networks with multiple internal states. *Cerebral Cortex* 16:639–654.

Gähwiler B (1981) Organotypic monolayer cultures of nervous tissue. *Journal of neuroscience methods* 4:329–342.

Gähwiler B (1988) Organotypic cultures of neural tissue. *Trends in neurosciences* 11:484–489.

García NVDM, Karayannis T, Fishell G (2011) Neuronal activity is required for the development of specific cortical interneuron subtypes. *Nature* 472:351–355.

Golowasch J, Abbott L, Marder E (1999) Activity-dependent regulation of potassium currents in an identified neuron of the stomatogastric ganglion of the crab cancer borealis. *Journal of Neuroscience* 19:RC33–1.

Grasselli G, He Q, Wan V, Adelman JP, Ohtsuki G, Hansel C (2016) Activity-dependent plasticity of spike pauses in cerebellar purkinje cells. *Cell reports* 14:2546–2553.

651 Graves AR, Moore SJ, Bloss EB, Mensh BD, Kath WL, Spruston N (2012) Hippocampal pyramidal neurons comprise

652 two distinct cell types that are countermodulated by metabotropic receptors. *Neuron* 76:776–789.

653 Hemond P, Epstein D, Boley A, Migliore M, Ascoli GA, Jaffe DB (2008) Distinct classes of pyramidal cells exhibit

654 mutually exclusive firing patterns in hippocampal area ca3b. *Hippocampus* 18:411–424.

655 Hille B (2001) *Ion channels of excitable membranes*, Vol. 507 Sinauer Sunderland, MA.

656 Hines ML, Carnevale NT (1997) The neuron simulation environment. *Neural computation* 9:1179–1209.

657 Hosp JA, Strüber M, Yanagawa Y, Obata K, Vida I, Jonas P, Bartos M (2014) Morpho-physiological criteria divide

658 dentate gyrus interneurons into classes. *Hippocampus* 24:189–203.

659 Hu H, Vervaeke K, Storm JF (2002) Two forms of electrical resonance at theta frequencies, generated by m-current,

660 h-current and persistent na+ current in rat hippocampal pyramidal cells. *The Journal of physiology* 545:783–805.

661 Hunt D, Linaro D, Si B, Romani S, Spruston N (2018) A novel pyramidal cell type promotes sharp-wave

662 synchronization in the hippocampus. *Nature neuroscience* .

663 Hutcheon B, Yarom Y (2000) Resonance, oscillation and the intrinsic frequency preferences of neurons. *Trends in*

664 *neurosciences* 23:216–222.

665 Hyun JH, Eom K, Lee KH, Ho WK, Lee SH (2013) Activity-dependent downregulation of d-type k+ channel subunit

666 kv1. 2 in rat hippocampal ca3 pyramidal neurons. *The Journal of physiology* 591:5525–5540.

667 Kapoor R, Jaeger C, Llinas R (1988) Electrophysiology of the mammalian cerebellar cortex in organ culture.

668 *Neuroscience* 26:493–507.

669 Keogh E, Ratanamahatana CA (2005) Exact indexing of dynamic time warping. *Knowledge and information*

670 *systems* 7:358–386.

671 Kim D, Song I, Keum S, Lee T, Jeong MJ, Kim SS, McEnery MW, Shin HS (2001) Lack of the burst firing

672 of thalamocortical relay neurons and resistance to absence seizures in mice lacking α 1g t-type ca 2+ channels.

673 *Neuron* 31:35–45.

674 Kochegarov AA (2003) Pharmacological modulators of voltage-gated calcium channels and their therapeutical
675 application. *Cell calcium* 33:145–162.

676 Kumaran D, Hassabis D, McClelland JL (2016) What learning systems do intelligent agents need? complementary
677 learning systems theory updated. *Trends in cognitive sciences* 20:512–534.

678 Lee PR, Cohen JE, Becker KG, Fields RD (2005) Gene expression in the conversion of early-phase to late-phase
679 long-term potentiation. *Annals of the New York Academy of Sciences* 1048:259–271.

680 Li B, Tadross MR, Tsien RW (2016) Sequential ionic and conformational signaling by calcium channels drives
681 neuronal gene expression. *Science* 351:863–867.

682 Llinás RR (1988) The intrinsic electrophysiological properties of mammalian neurons: insights into central nervous
683 system function. *Science* 242:1654–1664.

684 Luthi A, Gahwiler BH, Gerber U (1996) A slowly inactivating potassium current in ca3 pyramidal cells of rat
685 hippocampus in vitro. *Journal of Neuroscience* 16:586–594.

686 Mahon S, Charpier S (2012) Bidirectional plasticity of intrinsic excitability controls sensory inputs efficiency in layer
687 5 barrel cortex neurons in vivo. *Journal of Neuroscience* 32:11377–11389.

688 Marder E, Goaillard JM (2006) Variability, compensation and homeostasis in neuron and network function. *Nature*
689 *Reviews Neuroscience* 7:563–574.

690 Markram H, Toledo-Rodriguez M, Wang Y, Gupta A, Silberberg G, Wu C (2004) Interneurons of the neocortical
691 inhibitory system. *Nature Reviews Neuroscience* 5:793–807.

692 McCormick DA, Connors BW, Lighthall JW, Prince DA (1985) Comparative electrophysiology of pyramidal and
693 sparsely spiny stellate neurons of the neocortex. *Journal of neurophysiology* 54:782–806.

694 Miller MN, Okaty BW, Nelson SB (2008) Region-specific spike-frequency acceleration in layer 5 pyramidal neurons
695 mediated by kv1 subunits. *Journal of Neuroscience* 28:13716–13726.

Moody WJ, Bosma MM (2005) Ion channel development, spontaneous activity, and activity-dependent development in nerve and muscle cells. *Physiological reviews* 85:883–941.

Okamoto K, Ishikawa T, Abe R, Ishikawa D, Kobayashi C, Mizunuma M, Norimoto H, Matsuki N, Ikegaya Y (2014) Ex vivo cultured neuronal networks emit in vivo-like spontaneous activity. *The Journal of Physiological Sciences* 64:421–431.

Paz JT, Mahon S, Tiret P, Genet S, Delord B, Charpier S (2009) Multiple forms of activity-dependent intrinsic plasticity in layer v cortical neurones in vivo. *The Journal of physiology* 587:3189–3205.

Prescott SA, Ratté S, De Koninck Y, Sejnowski TJ (2008) Pyramidal neurons switch from integrators in vitro to resonators under in vivo-like conditions. *Journal of neurophysiology* 100:3030–3042.

Remme MW, Donato R, Mikiel-Hunter J, Ballestero JA, Foster S, Rinzel J, McAlpine D (2014) Subthreshold resonance properties contribute to the efficient coding of auditory spatial cues. *Proceedings of the National Academy of Sciences* 111:E2339–E2348.

Sánchez-Aguilera A, Sánchez-Alonso J, Vicente-Torres M, Colino A (2014) A novel short-term plasticity of intrinsic excitability in the hippocampal ca1 pyramidal cells. *The Journal of physiology* 592:2845–2864.

Saviane C, Mohajerani MH, Cherubini E (2003) An id-like current that is downregulated by ca2+ modulates information coding at ca3–ca3 synapses in the rat hippocampus. *The Journal of physiology* 552:513–524.

Schreiber S, Fellous JM, Tiesinga P, Sejnowski TJ (2004) Influence of ionic conductances on spike timing reliability of cortical neurons for suprathreshold rhythmic inputs. *Journal of neurophysiology* 91:194–205.

Sherman SM (2001) Tonic and burst firing: dual modes of thalamocortical relay. *Trends in neurosciences* 24:122–126.

Shin J, Koch C, Douglas R (1999) Adaptive neural coding dependent on the time-varying statistics of the somatic input current. *Neural computation* 11:1893–1913.

Somogyi P, Klausberger T (2005) Defined types of cortical interneurone structure space and spike timing in the hippocampus. *The Journal of physiology* 562:9–26.

Srikanth S, Narayanan R (2015) Variability in state-dependent plasticity of intrinsic properties during cell-autonomous self-regulation of calcium homeostasis in hippocampal model neurons. *eNeuro* 2:ENEURO–0053.

Stemmler M, Koch C (1999) How voltage-dependent conductances can adapt to maximize the information encoded by neuronal firing rate. *Nature neuroscience* 2:521–527.

Steriade M (2004) Neocortical cell classes are flexible entities. *Nature reviews neuroscience* 5:121–134.

Storm JF (1988) Temporal integration by a slowly inactivating k+ current in hippocampal neurons. *Nature* 336:379.

Su H, Sochivko D, Becker A, Chen J, Jiang Y, Yaari Y, Beck H (2002) Upregulation of a t-type ca2+ channel causes a long-lasting modification of neuronal firing mode after status epilepticus. *The Journal of neuroscience* 22:3645–3655.

Tasic B, Menon V, Nguyen TN, Kim TK, Jarsky T, Yao Z, Levi B, Gray LT, Sorensen SA, Dolbeare T et al. (2016) Adult mouse cortical cell taxonomy revealed by single cell transcriptomics. *Nature neuroscience* 19:335–346.

Thompson L, Moyer J, Disterhoft J (1996) Transient changes in excitability of rabbit ca3 neurons with a time course appropriate to support memory consolidation. *Journal of Neurophysiology* 76:1836–1849.

Titley HK, Brunel N, Hansel C (2017) Toward a neurocentric view of learning. *Neuron* 95:19–32.

Tricoire L, Pelkey KA, Erkkila BE, Jeffries BW, Yuan X, McBain CJ (2011) A blueprint for the spatiotemporal origins of mouse hippocampal interneuron diversity. *The Journal of Neuroscience* 31:10948–10970.

Turrigiano G, Abbott L, Marder E (1994) Activity-dependent changes in the intrinsic properties of cultured neurons. *Science-AAAS-Weekly Paper Edition-including Guide to Scientific Information* 264:974–976.

Turrigiano GG, Nelson SB (2004) Homeostatic plasticity in the developing nervous system. *Nature Reviews Neuroscience* 5:97–107.

Van Aerde KI, Feldmeyer D (2015) Morphological and physiological characterization of pyramidal neuron subtypes in rat medial prefrontal cortex. *Cerebral cortex* 25:788–805.

741   Ward Jr JH (1963) Hierarchical grouping to optimize an objective function. *Journal of the American statistical*

742   *association* 58:236–244.

743   Wu WW, Chan CS, Surmeier DJ, Disterhoft JF (2008) Coupling of l-type ca2+ channels to kv7/kcnq channels creates

744   a novel, activity-dependent, homeostatic intrinsic plasticity. *Journal of neurophysiology* 100:1897–1908.

745   Yao WD, Wu CF (2001) Distinct roles of camkii and pka in regulation of firing patterns and k+ currents in drosophila

746   neurons. *Journal of neurophysiology* 85:1384–1394.

747   Zhang W, Linden DJ (2003) The other side of the engram: experience-driven changes in neuronal intrinsic

748   excitability. *Nature Reviews Neuroscience* 4:885–900.